NASA CONTRACTOR REPORT

NASA CR-2580

2. 4/24

4.

DETERMINATION OF ROTOR HARMONIC BLADE LOADS FROM ACOUSTIC MEASUREMENTS, FINAL REPORT

Peter K. Kasper

Prepared by
3. WYLE LABORATORIES (S.)
Hampton, Va. 23666
for Langley Research Center
and U.S. Army Air Mobility R&D Laboratory

5.
NATIONAL AERONAUTICS AND SPACE ADMINISTRATION • WASHINGTON, D. C. • OCTOBER 1975

1. Report No.	2. Government Accession No.	3. Recipient's Catalog No.
NASA CR-2580		

4. Title and Subtitle	5. Report Date
DETERMINATION OF ROTOR HARMONIC BLADE LOADS FROM ACOUSTIC MEASUREMENTS	October 1975
	6. Performing Organization Code

7. Author(s)	8. Performing Organization Report No.
Peter K. Kasper	
	10. Work Unit No.

9. Performing Organization Name and Address	11. Contract or Grant No.
Wyle Laboratories 3200 Magruder Boulevard Hampton, Virginia 23666	NAS1-12390
	13. Type of Report and Period Covered
12. Sponsoring Agency Name and Address	Contractor Report
National Aeronautics and Space Administration Washington, D. C. 20546	14. Sponsoring Agency Code

15. Supplementary Notes

The contract research effort which has lead to the results in this report was financially supported by USAAMRDL (Langley Directorate).
Final report.

16. Abstract

The magnitude of discrete frequency sound radiated by a rotating blade is strongly influenced by the presence of a nonuniform distribution of aerodynamic forces over the rotor disk. When expressed in terms of a Fourier series in an angular position about the rotor axis, the nonuniform forces are commonly referred to as blade-load harmonics. Blade loading harmonic data has, in the past, been obtained from measurements of blade surface pressures using flush-mounted transducers rotating with the blade. The current study provides an analytical development and experimental results for a technique by which harmonic blade loads can be derived from acoustic measurements. The technique relates, on a one-to-one basis, the discrete frequency sound harmonic amplitudes measured at a point on the axis of rotation to the blade-load harmonic amplitudes. This technique was applied to acoustic data from two helicopter types and from a series of test results using the NASA-Langley Research Center rotor test facility. The inferred blade-load harmonics for the cases considered tended to follow an inverse power law relationship with harmonic blade-load number. Empirical curve fits to the data showed the harmonic fall-off rate to be in the range of 6 to 9 dB per octave of harmonic order. These empirical relationships were subsequently used as input data in a compatible far-field rotational noise prediction model. A comparison between predicted and measured off-axis sound harmonic levels is provided for the experimental cases considered.

17. Key Words (Suggested by Author(s))	18. Distribution Statement
Helicopter Noise, Rotor Rotational Noise, Harmonic Blade Loads, Rotor Noise Prediction, and Acoustic Measurements	Unclassified - Unlimited Subject category 71

19. Security Classif. (of this report)	20. Security Classif. (of this page)	21. No. of Pages	22. Price*
Unclassified	Unclassified	62	$4.25

TABLE OF CONTENTS

LIST OF ILLUSTRATIONS

LIST OF ILLUSTRATIONS (continued)

LIST OF ILLUSTRATIONS (continued)

LIST OF SYMBOLS

a	effective radius
B	number of blades
c	speed of sound
f_D	drag distribution function
F_D	total mean drag
F_D°	drag normalization constant
f_T	thrust distribution function
F_T	total mean thrust
F_T°	thrust normalization constant
g	monopole Green's function
g_ϕ	dipole Green's function for ϕ - component of force
g_z	dipole Green's function for z - component of force
i	$\sqrt{-1}$
$J_n(x)$	Bessel function of the first kind, order n, argument x
k	wavenumber = w/c
m	summation integer
M	effective rotational Mach number
n	summation integer
P	total acoustic pressure
P_D	drag-derived acoustic pressure component
P_s	amplitude of sth sound pressure harmonic

LIST OF SYMBOLS (continued)

P_T	thrust-derived acoustic pressure component
q	blade-load harmonic number
r	distance from rotor hub to observation point
r_o	radial distance on rotor disk
r_T	rotor disk radius
R	distance from source point to observation point
R_a	distance from observation point to effective radius
s	sound harmonic number
t	time
z	height of observation point
α_s	normalized chord load coefficient
β_q	normalized thrust load harmonic coefficient
γ_q	phase angle of qth harmonic component
δ_q	normalized drag load harmonic coefficient
$\delta( )$	Dirac delta function
θ	angle from vertical to observation point
ϕ	azimuthal angle to observation point
ϕ_o	azimuthal angle to source point
ω	angular blade-passing frequency = $B\Omega$
Ω	rotor shaft rotational speed

DETERMINATION OF ROTOR HARMONIC BLADE LOADS FROM ACOUSTIC MEASUREMENTS*

1.0 INTRODUCTION

The sound radiated by a rotating blade is characterized by a combination of broadband noise and discrete frequency noise. The noise spectra generated by the main rotor of a helicopter during normal operation are generally dominated by discrete frequencies below 500 Hz.

The radiation of discrete tones or rotational noise results from the cyclic interaction of aerodynamic forces on the acoustic media. The theoretical derivation of rotational noise due to a steady uniform force over a rotor disk is contained in a classic report by Gutin (Reference 1). In recent years, it has been recognized that magnitudes of the sound harmonics are primarily controlled by the presence of a nonuniform distribution of aerodynamic forces over the rotor disk. When expressed in terms of a Fourier series in angular position about the rotor axis, the nonuniform forces are commonly referred to as blade-load harmonics.

The magnitudes and frequency characteristics of the rotor harmonic blade loads have been studied experimentally by measuring the fluctuating pressures on the rotor blades with surface mounted pressure transducers. A recent report by Hosier and Ramakrishnan (Reference 2) contains a discussion of the experimental procedures and examples of typical surface pressure data. This direct measurement approach poses two major difficulties. One is the inherent experimental problem of recovering an electrical signal from a transducer rotating with the blade. The other difficulty relates to the conceptual problem of interpreting the net effect of measurements taken at isolated points along the blade. As discussed in Reference 2, the accuracy of rotational noise level predictions are dependent on the interpreted blade loading distribution.

The approach taken in this investigation was to deduce the blade-load harmonic amplitudes from measurements of the discrete frequency acoustic levels taken at a position on the rotor axis. The advantages of this approach

*The contract research effort which has led to the results in this report was jointly sponsored by NASA-Langley Research Center and USAAMRDL (Langley Directorate).

were that it required a less complicated measurement procedure and offers a direct means of determining the net effective harmonic loading.

The initial phase of the program was to undertake a review of current rotational noise theories. Theoretical approaches applicable to the blade methodology, presented in References 3 through 6 were reviewed in detail. The approach of Lowson and Ollerhead (Reference 3) consisted of modeling the acoustic properties of the rotor blade by means of a rotating point force. A solution to the three-dimensional wave equation was developed, expressing the radiated sound in terms of the harmonic blade-load components. The approaches of both Wright (References 4 and 5) and Morse and Ingard (Reference 6) consisted of modeling the forces applied to the acoustic media in terms of a distributed loading over the rotor disk. Wright utilized a formulation as developed by Lighthill to express the sound radiated by a dipole force distribution. Morse and Ingard took the mathematical approach of using a Green's function to relate the radiated sound pressures to blade-load forces. The solutions of both Wright, and Morse and Ingard can be compared with that of Lowson and Ollerhead by considering the source distribution as a concentrated loading at a given effective rotor radius. A comparison of the analytic expressions derived from these three approaches showed basic functional agreement.

Section 2.0 of this report provides a general presentation of the rotational noise theory utilized for calculations and predictions contained in the report. The theoretical section is divided into two parts. The first part provides the derivation of the relationship between on-axis acoustic harmonics and corresponding blade-load harmonics. The second part contains a derivation of the general rotational-noise prediction model using an approach similar to that of Reference 6.

Section 3.0 of the report provides a compilation of the blade-load harmonic values derived from acoustic measurements taken at the NASA-Langley Research Center for the following configurations:

a. OH-6 helicopter in hover at 24.4 meters (80 feet).

b. Bell 205 helicopter in hover at 24.4 meters (80 feet).

c. NASA LRC helicopter rotor test tower with a type UH1-D rotor blade.

Section 3.0 also contains a comparison of the measured off-axis sound harmonics with predictions based on the derived blade-load harmonic values. The conclusions of this investigation are contained in Section 4.0.

2.0 ROTATIONAL NOISE THEORY

As discussed in References 1 through 6, the acoustic source mechanism created by the interaction of a rotor blade with a fluid medium is dipole in nature. The aerodynamic forces within the rotor disk are described in terms of a continuous distribution of acoustic dipoles. The sound field due to this source distribution is derived by using the mathematical properties of a Green's function. As described in Reference 6, the Green's function corresponds to an expression for the acoustic pressure at an observation position due to a point source of unit strength located at a given source position. The total sound pressure due to a distributed acoustic source can then be determined by integrating the product of the Green's function and a source distribution function. To maintain a degree of simplicity in the mathematical model, the aerodynamic force distribution along the span of the rotor is taken to act at a single point. The model does, however, permit a consideration of the effect of loading variations across the chord of the rotor blade.

The theoretical treatment is applied first to derive the relationship between the near-field on-axis sound levels and the rotor blade-load thrust harmonics. Secondly, the general relationship between far-field sound harmonics and blade-load harmonics is derived.

2.1 Calculation of Harmonic Blade Loads from Axial Sound Harmonics

The radiation of discrete frequency sound from a rotating blade is a physical phenomenon exhibiting a complex dependence on phase. The following theoretical development models the effect of the rotating blades as a distribution of dipole forces acting on the plane surface enclosed by the blade tips. The sound pressure at an arbitrary observation point is the instantaneous sum of contributions from all points of the force distribution, each with appropriate phase. Mathematically, the expression for sound radiated along the rotor axis is simplified from the general expression for radiated sound. This simplification results because all sound radiated from points at a fixed blade radius arrive in phase at any observation point on the rotor axis. The forces acting on the rotor disk surface are taken to act at a given effective radius.

A diagram of the cylindrical coordinate system to be used for the derivation of the harmonic blade loads from axial sound harmonics is shown in Figure 1.

The forces acting on the rotor disk surface are taken to act at a single effective radius. The positive z-axis is the direction of blade thrust, and the blade is rotating in the direction of positive ω. Besides the approximations inherent in the point force concept, the analysis is otherwise exact in the classical sense, and therefore, provides both near-field and far-field results.

As discussed in Reference 7, the Green's function mathematically represents a solution to the Helmholtz equation expressing the spatial factor of a wave generated by a unit simple-harmonic point source. Using the coordinates of Figure 1, the Green's function for sound radiated along the rotor axis is given by

$$g = \frac{\exp(iskR)}{4\pi R} \qquad \text{(Eq. 1)}$$

where $R^2 = z^2 + r_o^2$

z = height of observation point above rotor

r_o = radial distance

k = wave number of fundamental sound harmonic

s = harmonic integer

The Green's function for sound radiated by a point dipole source is derived by taking the gradient of the simple point source function. For the force component in the z direction, the dipole Green's function thus becomes

$$g_z \equiv \frac{+\partial g}{\partial z} = \frac{iskz}{4\pi R^2} e^{iskR} - \frac{z}{4\pi R^3} e^{iskR} \qquad \text{(Eq. 2)}$$

Since the Green's function for sound along the axis is independent of ϕ, the contribution to sound radiation due to the drag component in the plane of the rotor disk is zero. That is

$$g_\phi \equiv -\frac{1}{r_o}\frac{\partial g}{\partial \phi} = 0 \qquad \text{(Eq. 3)}$$

The next item required is an expression for the distribution of force in the z direction over the rotor disk. As discussed in references 3 through 6, the force distribution over the rotor disk may be represented by a double Fourier series expressing periodic conditions in both time and in azimuthal angle ϕ_o. Using complex notation, the Fourier series can be put in the form

$$f_T = F_T^o \sum_{s,\,q=\infty}^{\infty} \alpha_s \beta_q \left[\exp\left(i\left(sB+q \right) \phi_o - is\omega t \right) \right] \delta\left(r_o - a \right) \qquad \text{(Eq. 4)}$$

where

f_T = thrust distribution

F_T^o = $\dfrac{\text{average thrust force}}{\text{length of circumference}}$

α_s = normalized chord load coefficient

β_q = normalized blade thrust load harmonic coefficient

s = sound harmonic number

B = number of blades

q = blade load harmonic number

$\delta(r_o - a)$ = Dirac delta function

a = effective radius

In general, the coefficients α_s and β_q are complex numbers. The coefficient α_s represents the normalized harmonic force component at a fixed point on the rotor disk due to the periodic passage of a rotor blade. The value of the coefficient α_s for a given harmonic number is a function of the rotor blade chord width, the blade repetition rate, and the chord loading distribution. At low sound harmonic frequencies where the acoustic wavelengths are much larger than the chord width, the coefficients approach unity. For the range of blade-load harmonics considered in this study, the effect of chord loading is neglected, and all the coefficients represented by α_s are set equal to unity.

The blade-loading coefficient β_q represents the periodic force component that is experienced at a position on the blade as it rotates through a time-independent, but nonuniform flow. The normalization of β_q is such that the steady or net thrust load β_o is equal to unity, and that each β_q with $q \neq o$ represents the ratio of the qth harmonic load to the steady load.

Using the mathematical properties of the Green's function, the acoustic pressure along the rotor axis is determined by integrating the product of the Green's function and the source distribution over the rotor disk, with radius r_T.

$$P = \int_o^{2\pi} \int_o^{r_T} f_T g_z r_o \, dr_o d\phi_o \qquad \text{(Eq. 5)}$$

Replacing f_T and g_z with the previously indicated expressions gives the equation

$$P = F_T^o \sum_{s,q=\infty}^{\infty} \exp(-is\omega t)\, \alpha_s \beta_q \int_o^{2\pi} \int_o^{r_T} \delta(r_o - a)$$

$$\times \left[\frac{iskz}{4\pi R^2} - \frac{z}{4\pi R^3}\right] \exp\left[i(sB+q)\phi_o + iskR\right] r_o dr_o d\phi_o \qquad \text{(Eq. 6)}$$

Next, using the property of the Dirac delta function, the integration over the radius of the rotor disk is given by

$$P = aF_T^o \sum_{s,q=-\infty}^{\infty} \left[\exp\left(iskR_a - is\omega t\right)\right]$$

$$\times\ \alpha_s \beta_q \left[\frac{iskz}{4\pi R_a^2} - \frac{z}{4\pi R_a^3}\right] \int_o^{2\pi} \exp\left(i(sB+q)\phi_o\right) d\phi_o \qquad \text{(Eq. 7)}$$

$$\text{with } R_a = \sqrt{z^2 + a^2}$$

Considerable simplification results from the ϕ_o integration. All terms in the double series are equal to zero except those in which sB equals -q. The remaining terms increase in amplitude by a factor of 2π:

$$P = 2\pi a F_T^o \sum_{s=-\infty}^{\infty} \alpha_s \beta_{-sB} \left[\frac{iskz}{4\pi R_a^2} - \frac{z}{4\pi R_a^3} \right] \exp\left(iskR_a - is\omega t \right) \qquad \text{(Eq. 8)}$$

To examine the physical significance of this expression, it is helpful to convert from complex to real notation. This is readily accomplished by first expressing β_{sB} in terms of an amplitude and a phase.

That is
$$\beta_{sB} = |\beta_{sB}| \exp\left(i\gamma_{sB} \right) \qquad \text{(Eq. 9a)}$$

By convention, the value β_{-sB} is similarly expressed as

$$\beta_{-sB} = |\beta_{sB}| \exp\left(-i\gamma_{sB} \right) \qquad \text{(Eq. 9b)}$$

If by some circumstance β_{sB} were a real quantity, it would represent a harmonic blade load which was symmetric about some diameter in the rotor disk. Conversely, if β_{sB} were purely imaginary, it would represent an antisymmetric blade load. To close approximation, the coefficients α_s represent a symmetric time dependence and will be taken as real values. The summation limits of Equation 8 are changed using the relationship

$$\sum_{n=-\infty}^{\infty} A_n = A_o + \sum_{n=1}^{\infty} \left(A_{-n} + A_n \right) \qquad \text{(Eq. 10)}$$

Rearranging terms and converting from exponential to trigonometric forms provides

$$P = 2\pi a F_T^o \sum_{s=1}^{\infty} 2\alpha_s |\beta_{sB}| \left\{ \frac{skz}{4\pi R_a^2} \sin \nu + \frac{z}{4\pi R_a^3} \cos \nu \right\} \qquad \text{(Eq. 11)}$$

where $\nu = skR_a - s\omega t - \gamma_{sB}$

The s = 0 term in the expression for P has been dropped since it corresponds to a DC pressure wave and does not contribute to the acoustic pressure. The coefficients of the sine and cosine terms in this series represent the far-field and near-field terms, respectively.

In practice, the quantities ultimately measured are the harmonic values of the mean-square pressure. Taking the mean-square value of the above series, equation 11 yields the following

$$\overline{P^2} = \sum_{s=1}^{\infty} \overline{P}^{2}_{rms} = 2F_T^2 \sum_{s=1}^{\infty} \alpha_s^2 |\theta_{sB}|^2 \left[\left(\frac{skz}{4\pi R_a^2} \right)^2 + \left(\frac{z}{4\pi R_a^3} \right)^2 \right] \quad \text{(Eq. 12)}$$

where F_T = total mean thrust = $2\pi a F_T^{\circ}$

P_s^{rms} = root-mean-square magnitude of acoustic harmonic component of harmonic number s

By equating the above series term-by-term, the magnitudes of the blade-load harmonics are solved in terms of the individual acoustic harmonics.

That is

$$|\theta_{sB}| = \frac{P_s^{rms}}{\sqrt{2}\, F_T \alpha_s} \left[\left(\frac{skz}{4\pi R_a^2} \right)^2 + \left(\frac{z}{4\pi R_a^3} \right)^2 \right]^{-1/2} \quad \text{(Eq. 13)}$$

For the special case of sound radiation along the rotor axis, each acoustic harmonic component is related to an individual blade-load harmonic. It is important to note from Equation 13 that the acoustic harmonic designated by integer s is related solely to the blade harmonic with harmonic number sB. Taking the example of a rotor with two blades, on-axis measurements of the acoustic harmonics could be used to determine only the even-numbered blade-loading harmonics. Also of importance, in the above expression, is the result that the relationship between on-axis acoustic harmonic and blade-load harmonics is independent of the blade-load harmonic phases.

2.2 Derivation of General Analytic Model

The theoretical development for the general case of sound radiation from a rotor disk is an extension of the analytic technique used in the previous section. In view of the greater complexity, it is necessary to make pertinent approximations to arrive at a tractable solution. The coordinate geometry used for the derivation is shown in Figure 2.

Proceeding as before, the initial step is to develop a functional form for the Green's function. As detailed in Reference 6, the contribution at any observation point due to a unit point source in the plane of the rotor disk is given by

$$g = \frac{1}{4\pi} \frac{\exp\left(isk\left|\vec{r}-\vec{r}_o\right|\right)}{\left|\vec{r}-\vec{r}_o\right|} \qquad \text{(Eq. 14)}$$

where the vectors $\vec{r}$ and $\vec{r}_o$ represent the spherical coordinate points (r, θ, ϕ) and $\left(r_o, \frac{\pi}{2}, \phi_o\right)$, respectively. By limiting our considerations to the far-field case where $r >> r_o$, the distance $\left|\vec{r}-\vec{r}_o\right|$ is approximated by the following expression

$$\left|\vec{r}-\vec{r}_o\right| \simeq r - r_o \sin\theta \cos\left(\phi-\phi_o\right) \qquad \text{(Eq. 15)}$$

Accordingly, the Green's function is then approximated by

$$g = \frac{1}{4\pi r} \exp\left[iskr - iskr_o \sin\theta \cos\left(\phi-\phi_o\right)\right] \qquad \text{(Eq. 16)}$$

The exponential form is expanded in a Fourier series using the relationship

$$\exp\left[iskr_o \sin\theta\cos\left(\phi-\phi_o\right)\right] = \sum_{m=-\infty}^{\infty} i^m J_m\left(skr_o\sin\theta\right) \exp\left(im\left(\phi-\phi_o\right)\right) \qquad \text{(Eq. 17)}$$

The point source Green's function then becomes

$$g = \frac{1}{4\pi r} \exp(iskr) \sum_{m=-\infty}^{\infty} i^m J_m(skr_o \sin\theta) \left[\exp\left(im(\phi - \phi_o)\right)\right] \qquad \text{(Eq. 18)}$$

As in the previous section, the net reaction forces on the acoustic media due to thrust and drag forces is represented as a distribution of dipoles over the rotor disk. The Green's functions representing the pressure contributions from thrust and drag dipole orientations are given as follows

$$g_z = \frac{\partial g}{\partial z} = \frac{\partial g}{\partial r} \cos\theta = \frac{iskcos\theta exp(iskr)}{4\pi r} \sum_{m=-\infty}^{\infty} i^m J_m(skr_o \sin\theta) \exp\left(im(\phi - \phi_o)\right)$$

(Eq. 19)

$$g_\phi = -\frac{1}{r_o} \frac{\partial g}{\partial \phi} = \frac{i}{r_o} \left(\exp(iskr) / 4\pi r\right) \sum_{m=-\infty}^{\infty} mi^m J_m(skr_o \sin\theta) \exp\left(im(\theta - \theta_o)\right)$$

(Eq. 20)

As before, the actual distribution of force over the rotor disk is modeled as acting about a ring of effective radius a. Using the previous expression for thrust distribution f_T, the sound contribution from the thrust distribution is expressed as

$$P_T = \int_o^{2\pi} \int_o^{r_T} f_T g_z r_o dr_o d\phi_o = \frac{ikcos\theta}{4\pi r} \cdot \sum_{s,m,q=-\infty}^{\infty} i^m s \int_o^{2\pi} \int_o^{r_T} F_T^o \alpha_s \beta_q x$$

$$J_m(skr_o \sin\theta) \exp\left[i(sB+q)\phi_o - is\omega t + im(\phi - \phi_o)\right] \delta(r - r_o) r_o dr_o d\phi_o$$

(Eq. 21)

The ϕ_o integration yields zero terms except for $m = sB + q$, thereby eliminating the summation over integer m. The integration over the Dirac delta function finally provides the expression

$$P_T = 2\pi a F_T^o \frac{\cos\theta}{4\pi r} \sum_{s,q=-\infty}^{\infty} \text{ski}^{(sB+q)+1} \alpha_s \beta_q J_{sB+q}(ska \sin\theta)$$

$$\times \exp\left[iskr + i(sB+q)\phi - is\omega t\right] \qquad \text{(Eq. 22)}$$

The derivation of an acoustic pressure component due to dipole drag forces proceeds in a similar fashion. The drag-force distribution is taken, as expressed in the following equation, to act at the same effective radius (a) as the thrust distribution

$$f_D = F_D^o \sum_{s,q=-\infty}^{\infty} \alpha_s \delta_q \left(\exp\left[i(sB+q)\phi_o - is\omega t\right]\right) \delta(r_o - a) \qquad \text{(Eq. 23)}$$

$$\text{where} \quad F_D^o = \frac{\text{Average Drag Force}}{\text{Length at Circumference}} = \frac{F_D}{2\pi a}$$

Utilizing the properties of the Green's function

$$P_D = \int_o^{2\pi} \int_o^{r_T} g_\phi f_D r_o dr_o d\phi_o \qquad \text{(Eq. 24)}$$

Performing the indicated integration yields

$$P_D = \frac{F_D}{4\pi ra} \sum_{s,q=-\infty}^{\infty} i^{(sB+q)+1} (sB+q) \alpha_s \delta_q J_{sB+q}(ska \sin\theta)$$

$$\times \exp\left[iskr + i(sB+q) - is\omega t\right] \qquad \text{(Eq. 25)}$$

Note that the harmonic drag coefficients δ_q, like the thrust coefficients β_q, are in general complex values. Without much loss in generality, some simplification is achieved by taking the phases of the drag harmonics to be identical with those of the thrust harmonics. Mathematically,

$$\delta_q = |\delta_q| \exp(i\gamma_q) \qquad \text{(Eq. 26a)}$$

and

$$\delta_{-q} = |\delta_q| \exp(-i\gamma_q) \qquad \text{(Eq. 26b)}$$

The expression for the total acoustic pressure at an arbitrary far-field reference point is given by the instantaneous addition of the thrust and drag-derived component pressures

$$P = P_T + P_D \qquad \text{(Eq. 27)}$$

Combining the expressions for P_T and P_D results in

$$P = \frac{1}{4\pi r} \sum_{s,\,q=\infty}^{\infty} \left[-skf_t |\beta_q| \cos\theta + F_D |\delta_q| \frac{(sB+q)}{a}\right] \alpha_s J_{sB+q}(ska \sin\theta)$$

$$\times \exp\left[iskr + i(sB+q)\left(\phi + \frac{\pi}{2}\right) + i\gamma_q - is\omega t\right] \qquad \text{(Eq. 28)}$$

By expanding the series and regrouping terms, it can be shown that with the use of the expression $J_n(Z) = J_{-n}(-Z)$, the series for P can be changed to the following trigonometric form

$$P = \frac{1}{4\pi r} \sum_{s=1}^{\infty} 2\alpha_s \left\{ \sum_{q=0}^{\infty} \left[-skF_T |\beta_q| \cos\theta + F_D |\delta_q| \frac{(sB-q)}{a}\right] J_{sB-q}(ska \sin\theta) \right.$$

$$\left. \times \sin\psi_- + \sum_{q=0}^{\infty} \left[-skF_T |\beta_q| \cos\theta + F_D |\delta_q| \frac{(sB+q)}{a}\right] J_{sB+q}(ska \sin\theta) \sin\psi_+ \right\} \qquad \text{(Eq. 29)}$$

where $\psi_- = sk(r-ct) + (sB-q)(\phi + \frac{\pi}{2}) + \gamma_q$

$\psi_+ = sk(r-ct) + (sB+q)(\phi + \frac{\pi}{2}) + \gamma_q$ (Eq. 29) cont.

As discussed in References 3 and 6, the characteristics of Bessel functions related to the relative magnitude of the argument and the order may be used to make a simplifying approximation to the above equation. It is convenient to first express the argument of the Bessel function as

$$ska\sin\theta = sBM\sin\theta$$

where M = effective rotational Mach number = $\left(\frac{\omega}{B}\right)\frac{a}{c}$ (Eq. 30)

For typical helicopter operations, this rotational Mach number is less than unity. The absolute magnitude of the argument is then always less than the integer value sB. For these conditions, the magnitude of the J_{sB+q} functions is much smaller than the magnitude of the J_{sB-q} functions. For the calculations made in this study, the small contributions due to terms with a factor of J_{sB+q} were neglected.

The asymptotic properties of the Bessel functions were also used to set a limit on the number of terms included in the summation over the blade-load harmonic number q. The sum criteria recommended in Reference 3 is to include only the terms that satisfy the criteria

$$sB(1-M) \leq q \leq sB(1+M) \qquad \text{(Eq. 31)}$$

This criteria is strictly true only for a relatively flat blade-loading spectrum. For the calculations in this study, the lower limit of this criteria was removed.

The expression for the time-varying pressure is finally written

$$P = \frac{1}{4\pi r}\sum_{s=1}^{\infty}\sum_{q=0}^{\infty} 2\alpha_s \left[-skF_T|\beta_q|\cos\theta + F_D|\delta_q|\frac{(sB-q)}{a}\right] \qquad \text{(Eq. 32)}$$

$$\times J_{sB-q}(sBM\sin\theta)\sin\left[sk\,(r-ct) + (sB-q)\left(\phi+\frac{\pi}{2}\right)+\gamma_q\right] \qquad \text{(Eq. 32)}$$

To compare predicted values with measured values, it is necessary to transform this expression to indicate mean-square harmonic amplitudes. The mathematical process of taking the time-average value of the squared pressure yields the expression

$$\overline{P_s^2} = \frac{2\alpha_s^2}{(4\pi r)^2}\left\{\sum_{n=0}^{\infty}\sum_{q=0}^{\infty}\left[-skF_T|\beta_n|\cos\theta + F_D\,\frac{(sB-n)}{a}\,|\delta_n|\right]\right.$$

$$\times\left[-\,skF_T|\beta_q|\cos\theta + F_D\,\frac{(sB-q)}{a}\,|\delta_q|\right] J_{sB-n}(sBM\sin\theta)$$

$$\left.\times\, J_{sB-q}(sBM\sin\theta)\cos\left[\left(\phi+\frac{\pi}{2}\right)(n-q) + \gamma_n - \gamma_q\right]\right\} \qquad \text{(Eq. 33)}$$

To make use of this general expression, it is necessary to specify each of the individual blade-load phases γ_q as well as the harmonic amplitudes.

An alternative, discussed in detail in Reference 3, is to assume that the phase amplitudes vary randomly in time. The time-averaged harmonic pressure amplitudes then become independent of the azimuthal variable ϕ and is expressed as

$$\overline{P_s^2} = \frac{2\alpha_s^2}{(4\pi r)^2}\sum_{q=0}^{\infty}\left[-skF_T|\beta_q|\cos\theta + F_D\,\frac{(sB-q)}{a}\,|\delta_q|\right]^2$$

$$\times\, J_{sB-q}^2(sBM\sin\theta) \qquad \text{(Eq. 34)}$$

3.0 CALCULATED AND MEASURED RESULTS

The approach of determining blade loads from on-axis acoustic measurements was investigated experimentally using both actual helicopter data and rotor tower test data. For each test series, the sound levels at a position on the rotor axis were spectrally analyzed to obtain a set of sound harmonic amplitudes. These sound harmonics were used with Equation 13 of Section 2.1 to calculate rotor blade-load harmonic amplitudes. A least-squares curve fit was applied to the calculated blade-load harmonics to obtain an empirical relationship between harmonic number and amplitude. To test the utility of the empirical blade-load harmonic equations, they were used with the simplified random phase, rotational-noise prediction model (Equation 34) to calculate off-axis sound levels. These calculated sound levels were then compared with measured off-axis sound levels. The calculated and measured results are provided in the following report sections.

3.1 Helicopter Test Series

The helicopter noise data were obtained from a NASA-Langley noise measurement program in which the NASA Lunar Lander structure was used to position microphones about a helicopter in hover. Figure 3 is an illustration of the measurement configuration, showing the relative position of the helicopter to the microphone locations. Data were available from noise measurements of a four-bladed Hughes OH-6 helicopter and a two-bladed Bell 205 helicopter shown in Figures 4 and 5, respectively. For the helicopter noise measurements presented in this report, each helicopter was maintained in a hover at an altitude of 24.4 meters (80 feet). In view of the height of the helicopter and microphone positions above ground, it was anticipated that although ground reflection interference of sound waves can occur, the effect will be a small perturbation and was consequently neglected.

A block diagram of the instrumentation used to obtain the acoustic data is provided in Figure 6. The measurements were initially recorded on magnetic tape and subsequently processed using the SD 301C spectrum analyzer in the 0 to 500-Hz range with a 1.5-Hz bandwidth. The rms amplitudes of the rotational sound harmonics were read directly from the narrow band acoustic spectra. The microphone and signal amplification instrumentation provided a uniform frequency response from 20 Hz to 10kHz. Below 20 Hz, however, the system gain dropped sharply due primarily to the low-frequency response of the General Radio sound-level meter. The measured acoustic spectra obtained for the Bell helicopter tests showed that the first sound harmonic occurred at approximately 10 Hz. The amplitude of the first sound harmonic for these cases was consequently adjusted by 8 dB to account for the frequency response of the measurement system.

The sound harmonic amplitudes measured at 42.7 meters (140 feet) directly overhead of the helicopter were used in Equation 13 to calculate blade-load harmonic amplitudes. For these calculations, the chord-loading coefficients α_s, were taken to be unity, and the effective radius taken to act at the 85% radial station. Since the helicopter was in a stationary hover, the total upward thrust was taken to be equal to the gross helicopter weight.

The calculated blade-load harmonics for the OH-6 helicopter are shown in Figure 7. For the Bell 205 measurements, reliable data sets were available for two helicopter weight conditions, termed "low fuel" and "full fuel". The calculated blade-load harmonics for these two cases are shown in Figures 8 and 9. As seen in Figures 7 through 9, the calculated blade-load harmonics tend to cluster about a straight line when plotted in a full log format. The straight line indicated in each of these figures was determined from a least-squares curve fit of the data points, and in the equation form shown represents an inverse power law relationship. In terms of decibel notation, the indicated decrease of blade-load harmonic amplitude with increasing harmonic number corresponds to a fall-off rate of approximately 6 dB/octave for the OH-6 helicopter test case and approximately 8 dB/octave for the two Bell 205 helicopter test cases.

As a test of the empirical blade-load harmonic equations, they were used as input data in a prediction model to calculate off-axis sound levels. The radomized phase prediction model (Equation 34) was selected since the procedure used to determine the blade-load harmonic amplitudes does not provide any information about the loading harmonic phase angles. In addition, as discussed in References 2 and 3, the phase angle appears to be important only for the lowest order harmonics. Based on helicopter performance data, the ratio of total drag to total thrust was calculated to be 0.104 for the OH-6, 0.096 for the low-fuel Bell 205, and 0.106 for the full-fuel Bell 205 helicopter test cases. Therefore, in the prediction model, each blade-drag harmonic amplitude $F_{D\,\delta_q}$ was taken to be 0.1 of the corresponding blade-thrust harmonic amplitude $F_{T\,\beta_q}$.

The calculated directivity patterns for a sampling of the OH-6 rotational sound harmonic levels at a 52.1-meter (171-foot) radius is shown in Figure 10. Also plotted in this figure are the measured sound harmonic levels normalized to a 52.1-meter (171-foot) distance by accounting for spherical spreading. The deviation between measured and calculated sound levels for the overhead microphone position is due to the errors in approximating the determined blade loads by the empirical power law equation. Figure 10 shows that the theoretical model for the OH-6 test configuration predicts a sharp drop in the

harmonic sound levels for elevation angles between 70°and 90°. As shown, the measured harmonic levels at the 73°elevation are consistently higher than the calculated levels. The measured levels at the 36°elevation do, however, show scatter about the predicted values. These characteristics are also seen in the data for the "full-fuel" Bell 205 helicopter as shown in Figure 11.

A direct comparison of calculated and measured sound harmonic amplitudes for a range of harmonic numbers is presented in Figures 12 through 14 for the OH-6, "full-fuel" Bell 205, and "low-fuel" Bell 205 test cases, respectively. The missing data points in these figures were cases in which a tail rotor sound harmonic partially masked a main rotor sound harmonic.

3.2 Rotor Tower Test Series

In addition to the helicopter noise measurements, acoustic data were also obtained from a series of tests using the NASA-Langley Research Center helicopter rotor test facility pictured in Figure 15. The test series, identified as rotor tower test 12-A, was conducted with a two-bladed type UH-1D rotor. A sketch of the rotor test facility showing the relative microphone locations is provided in Figure 16. The on-axis microphone was suspended directly above the rotor hub from a horizontal overhead cable. For the test series, the UH-1D rotor was operated at various pitch angles and rotational speeds. Data from six different rotor conditions were chosen for detailed study for this investigation. Using the measured on-axis sound harmonic amplitudes as data input, Equation 13 was used to calculate the blade-load harmonic values. The calculated values for the six data sets are shown in Figures 17 through 22. As shown on each of these figures, a least-squares curve fit was performed to establish an empirical power law relationship for the blade-load harmonic values. These empirical relationships were then used with the rotational noise mathematical model to predict sound levels to be compared with the off-axis acoustic measurements.

To provide an indication of the theoretical directivity pattern, calculations were made of a sampling of sound harmonics as a function of elevation angle for one of the test runs. These harmonic levels were calculated for a 76.2-meter (250-foot) radius and are compared in Figure 23 with measured values adjusted for differences in spherical spreading.

From the location of the off-axis microphones at $\theta = 90^{\circ}$ and $\theta = 99.6^{\circ}$, the measured results were indicative of sound radiated in and near the plane of the rotor disk. Examination of the prediction model (Equation 34) shows

that for observation angles θ near 90°, the sound levels will be controlled by the blade-drag harmonic amplitudes. For the sound harmonic calculations, as done for the helicopter cases, the blade-drag harmonic amplitudes were taken to be 0.1 of the thrust harmonic amplitudes. Since the initial calculations showed a general tendency to underestimate the measured sound levels, the calculation procedure was repeated with the harmonic drag-to-thrust ratio increased to 0.2. A comparison of the calculated and measured sound harmonics for these cases is provided in Figures 24 to 29. For comparative purposes, the experimentally derived net drag-to-thrust ratio was also determined. Using the thrust and torque values measured on the rotor shaft, estimates of the net drag-to-thrust ratio were made by assuming the net drag force to act at the 85% radial station. For the rotor test facility cases considered, these net drag-to-thrust ratios were in the range 0.0625 to 0.0645. Use of these values would result in a decrease of predicted sound harmonic levels of up to 4 dB.

In view of the proximity of the rotor and microphone locations to the ground, it is likely that the ground reflected sound has had an effect on the measured data. A precise accounting of the effects of ground reflection would require details of the actual spatial distribution and acoustic directivity of the rotational noise source, as well as information about the acoustic impedance of the ground surface. Some indication of the effect of ground reflection can be seen, however, by comparing trends in the measured data with results calculated for the idealized configuration of an acoustic point source situated over an infinite rigid plane. A calculation of the interference pattern caused by ground reflections for this ideal case was made using the analytical procedure detailed in Reference 7.

The calculated interference patterns are shown in Figure 30 for sound harmonics based on a rotor rpm of 324. As seen in the top part of this figure, the in-plane microphone position is likely to exhibit the greatest interference effect. By comparison with Figures 26 through 29 for tests with similar rotor rpm, the measured in-plane data clearly shows the superimposed interference characteristic, particularly near sound harmonic numbers of 3 and 10. For the microphone position 0.8 meter (2.5 feet) above ground, the first calculated interference dip occurs well above the 20th sound harmonic number. Figure 30 shows the effect of a rigid reflecting surface for this configuration would be to add nearly 6 dB to the direct radiated sound. For the case of the overhead microphone position, as inidcated at the bottom of Figure 30, the reflected sound causes and interference pattern with a variation of within $\pm$1 dB.

Because of the ground cover, the interference effects caused by the actual ground reflection conditions at the helicopter rotor test facility are not likely to be as predominate as the ideal case considered here. Therefore, no corrections for ground reflections were applied to the predicted data so as not to obscure the prediction trends by an oversimplified set of factors.

4.0 CONCLUSIONS

The current study has provided a theoretical basis by which rotor-blade harmonic loading can be inferred by near-field as well as far-field acoustic measurements along the rotor axis. This analytic methodology has been applied to a variety of experimental cases involving noise measurements from two helicopter types as well as measurements taken during a series of static test facility runs.

The derived blade-load harmonics for the helicopter and rotor test facility cases considered have shown a reasonable fit to a simple harmonic number power law expression. When expressed in decibel form, these power law expressions provide decay rates of blade-load harmonic amplitudes with harmonic number in terms of dB/octave. A comparison of the blade-load harmonic decay rates determined from data in this report and decay rates discussed by other investigators is shown in Table I. It was anticipated that air flow recirculation effects during operation of the rotor test facility might possibly result in a harmonic blade load characteristic significantly different from that during a helicopter in hover. From a comparison of the experimental results summarized in Table I, it is apparent that the blade-load harmonic decay rates from both the helicopter and rotor test facility data fell within the range of 6 to 9 dB/octave. This is comparable to the 7 to 10 dB/octave decay reported by Hosier and Ramakrishnan (Reference 2). As shown in Table I, the derived decay rates fall within the transition range between impulsive and nonimpulsive noise conditions reported by Bausch, Munch and Schlegel (Reference 8). Similarly, the derived results also fall between the values suggestive of blade slap and smooth inflow predicted by Lowson and Ollerhead (Reference 3).

The acoustic predictions based on the empirically-derived blade loading power law relationships in conjunction with the random-phase prediction model were of only limited success. For the helicopter cases considered, the predicted values were within about 5 decibels of the measured values for the measurement location at 36° from the vertical axis. For the measurement location at 78°, the predicted sound harmonic levels were on the order of 10 dB lower than the measured values. This tendency of underestimating the sound levels for positions near the plane of the rotor was also evident from the rotor test facility data. The predicted sound harmonic for the $\theta = 90^{\circ}$ and $\theta = 99.6^{\circ}$ microphone positions were generally well below the measured values.

There are several potential reasons for the lack of correlation between the measured and predicted data. From an experimental standpoint, possible

explanations include acoustic measurement anomalies due to effects of ground reflection and the influence of micrometeorological conditions along the sound propagation path. Potential analytical explanations include prediction error due to the mathematical approximations inherent in the model and to the simplifications achieved by treating the loading forces in terms of a concentrated ring source. An explanation which does correspond to the general data trends is that, in addition to the anticipated dipole rotational noise radiation, there was a significant contribution to the measured data from the monopole rotational noise source referred to as blade-thickness noise. As discussed in References 9 and 10, blade-thickness noise is caused by the periodic displacement of fluid due to passage of the rotor blade. Although blade-thickness noise has generally been recognized as a source of less importance for subsonic rotor tip speeds, the sound directivity pattern does peak in the plane of the rotor disk.

REFERENCES

1. Gutin, L., "On the Sound Field of a Rotating Propeller," NASA Technical Memorandum 1195, 1948. (Translation)

2. Hosier, R. N. and Ramakrishnan, R., "Helicopter Rotor Rotational Noise Predictions based on Measured High-Frequency," presented at the 30th Annual National Forum of the American Helicopter Society, Washington, D.C., May 1974.

3. Lowson, M. V., Ollerhead, J. B., "Studies of Helicopter Rotor Noise," Wyle Laboratories Research Staff Report WR 68-9, USAAVLABS Technical Report 68-60, Fort Eustis, Va., January 1969.

4. Wright, S. E., "Sound Radiation From a Lifting Rotor Generated by Asymmetric Disk Loading," Journal of Sound and Vibration, 9, pp. 223-240, 1969.

5. Wright, S. E., "Discrete Radiation From Rotating Periodic Sources," Journal of Sound and Vibration, 17, pp. 437-498, 1971.

6. Morse, P. M., and Ingard, K. U., "Theoretical Acoustics," New York, McGraw-Hill Book Company, 1968.

7. Griffith, E. D., and Revell, "Low Noise Propeller Technology," (Appendix III), Air Force Aero Propulsion Laboratory, Technical Report AFAPL-TR-73-115, December 1973.

8. Bausch, W. P., Munch, C. L., and Schlegel, R. G., "An Experimental Study of Helicopter Rotor Impulsive Noise," USAAVLABS Technical Report 70-72, June 1971.

9. Farassat, F., "The Acoustic Far-Field of Rigid Bodies in Arbitrary Motion," Journal of Sound and Vibration, 32, 3, 387-405, 1974.

10. Lowson, M. V., "The Sound Field for Singularities in Motion," Proceedings of the Royal Society of London, Series A, 286, 559-572, 1965.

TABLE I

Data Source	Blade-Load Harmonic Fall-off Rate dB/Octave	Remarks
Figure 7	6	OH-6 in hover
Figures 8 and 9	8	Bell 205 in hover
Figures 17 to 22	6.5 to 9	Rotor test facility with UH 1-D blade
Hosier and Ramakrishnan (Reference 2)	7 to 10	Rotor test facility with four-bladed hingeless rotor
Bausch, Munch and Schlegel (Reference 8)	8.5 to 9.5	Nonimpulsive noise conditions
Bausch, Munch and Schlegel (Reference 8)	3.5	Impulsive noise conditions
Lowson and Ollerhead (Reference 3)	15	Predicted for smooth inflow
Lowson and Ollerhead (Reference 3)	0 to 6	Suggested for blade slap conditions

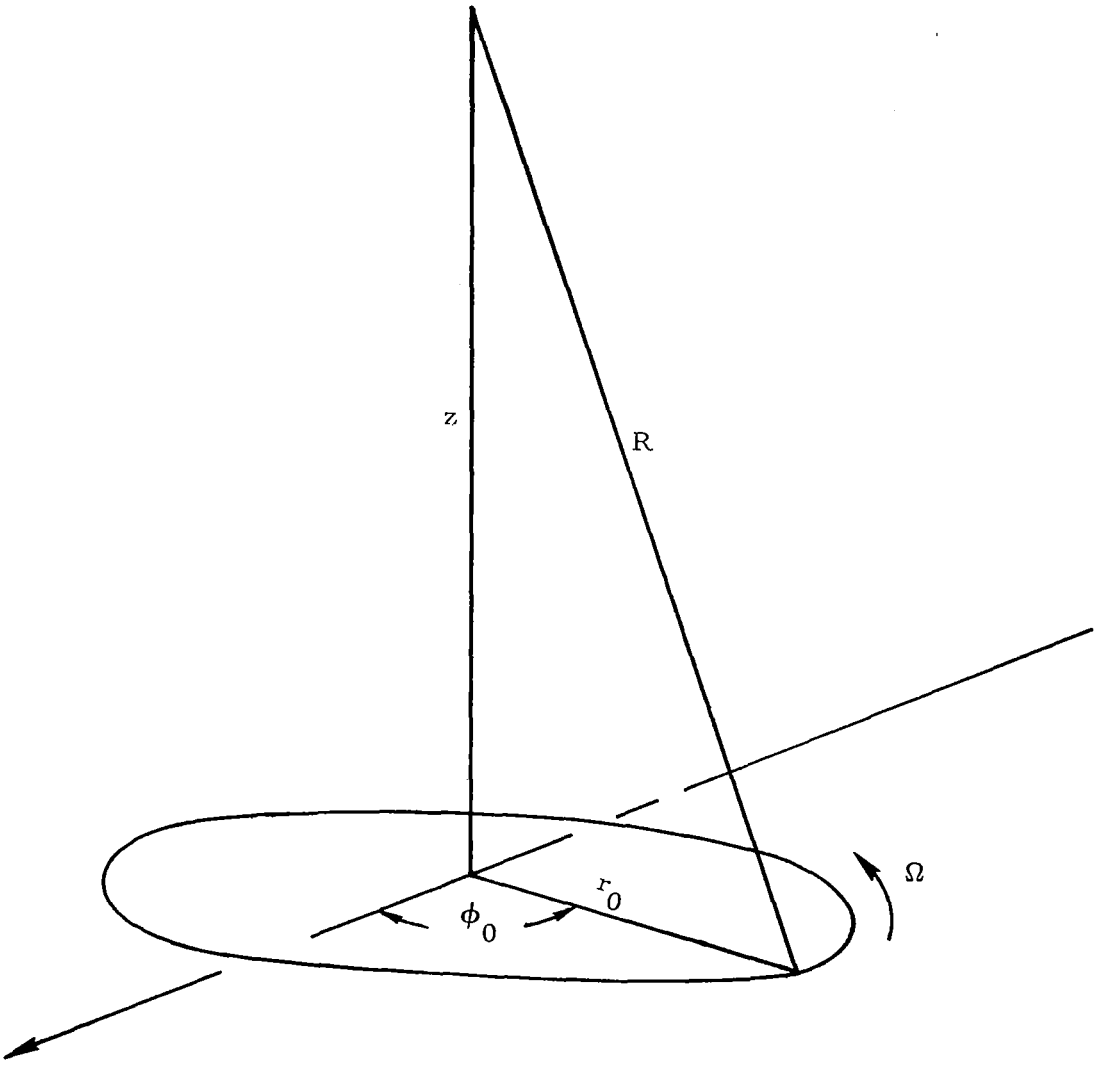

Figure 1. Coordinate System Used for Derivation of Axial Sound Harmonic to Blade-Load Harmonic Relationship

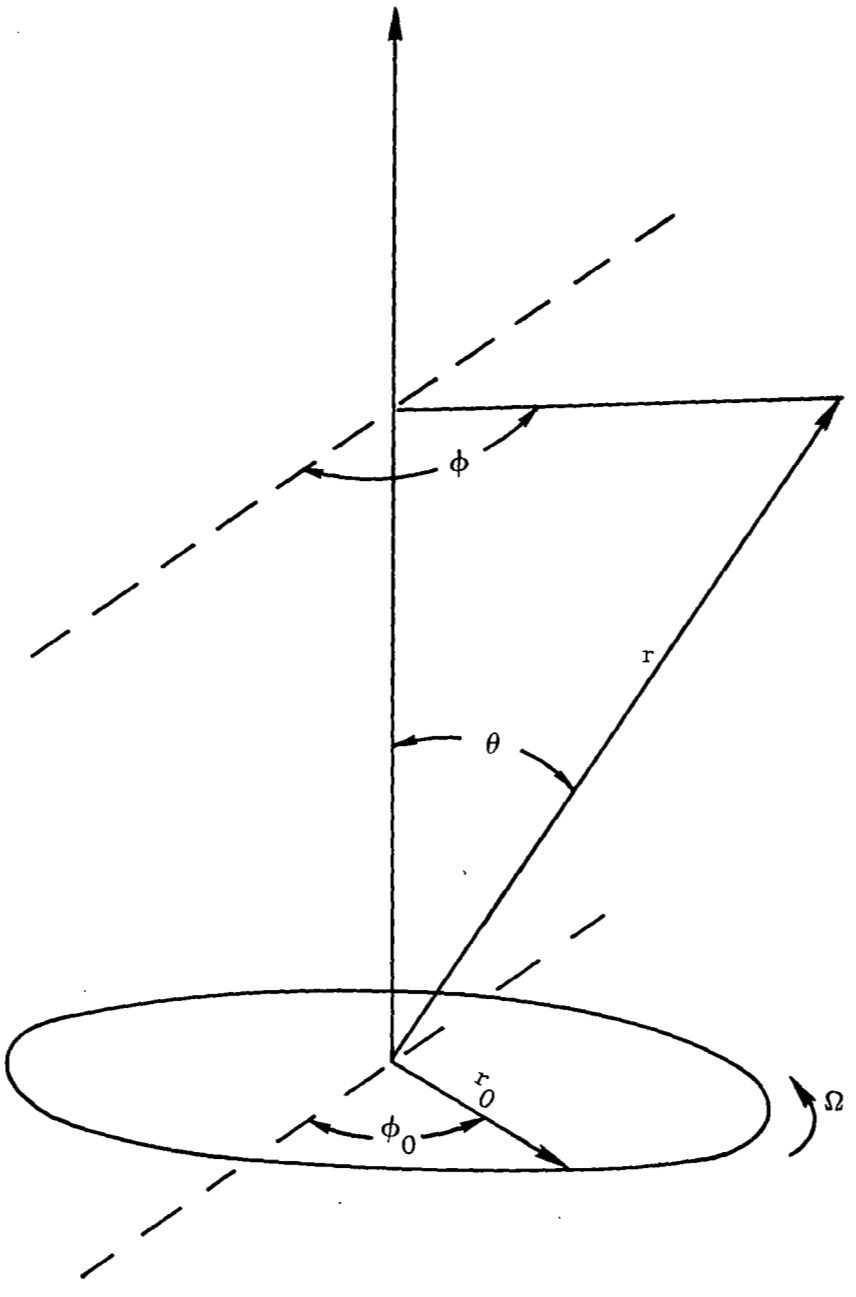

Figure 2. Coordinate System Used for Derivation of General Analytic Model

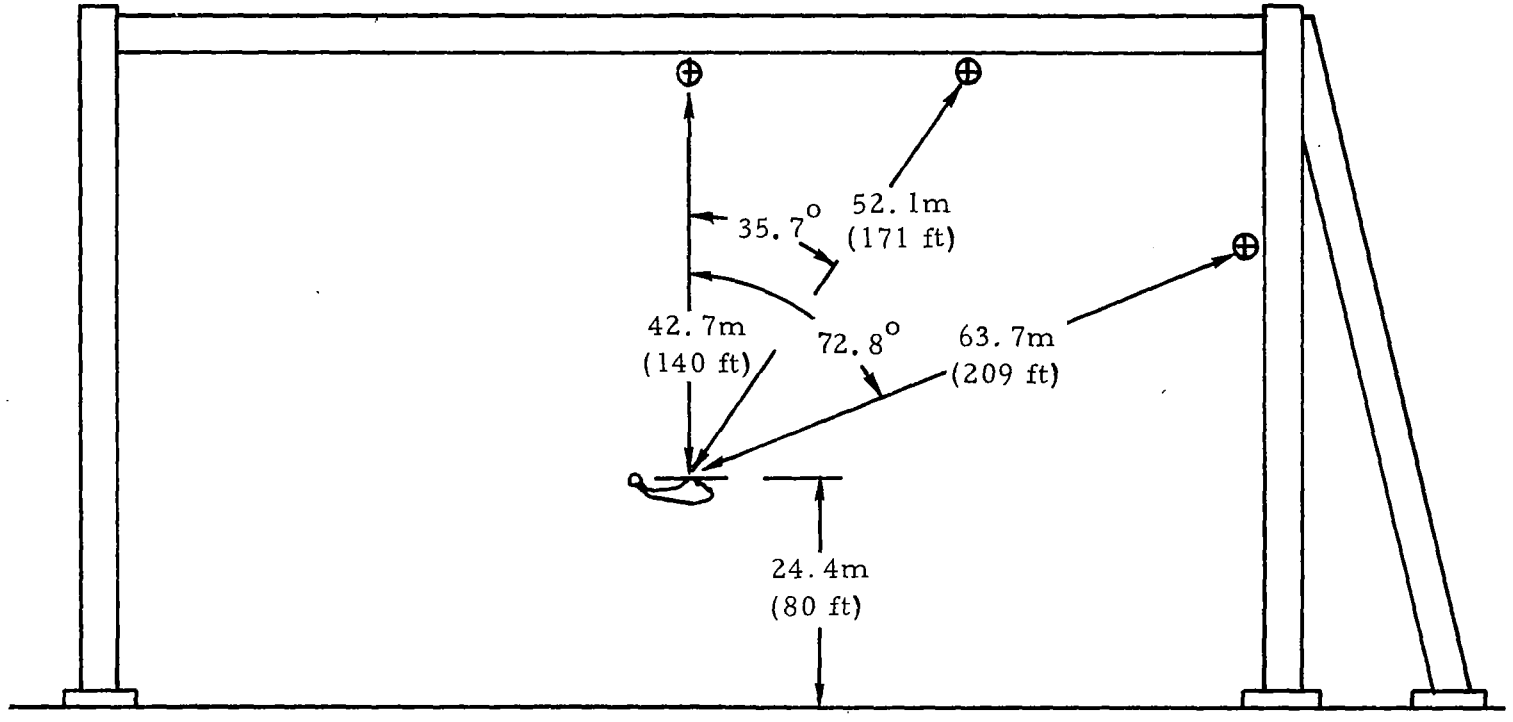

Figure 3. Microphone Locations Relative to Hovering Helicopter for Lunar Lander Test Series

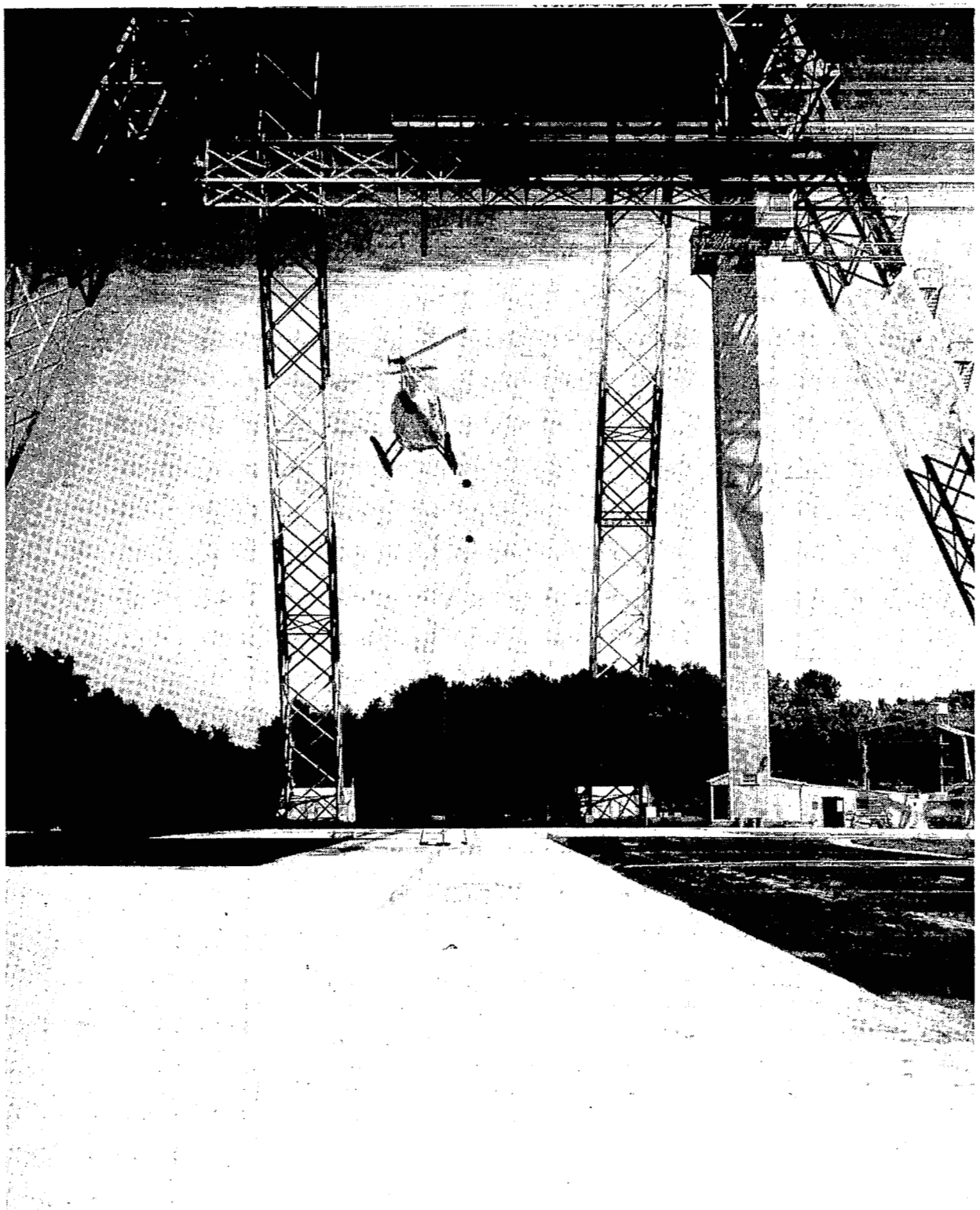

Figure 4. Hughes OH-6 Helicopter

Figure 5. Bell 205 Helicopter

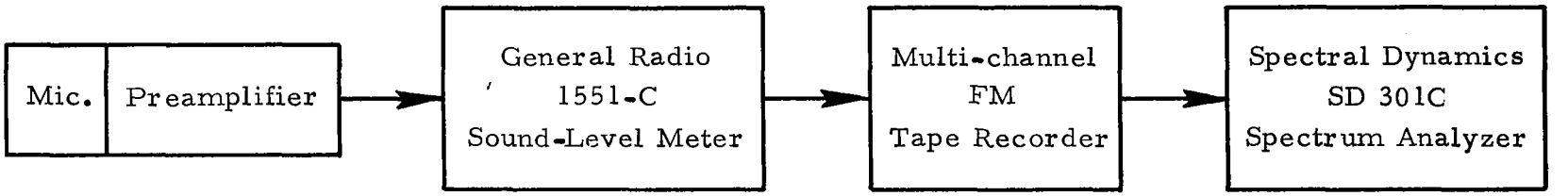

Figure 6. Instrumentation Block Diagram.

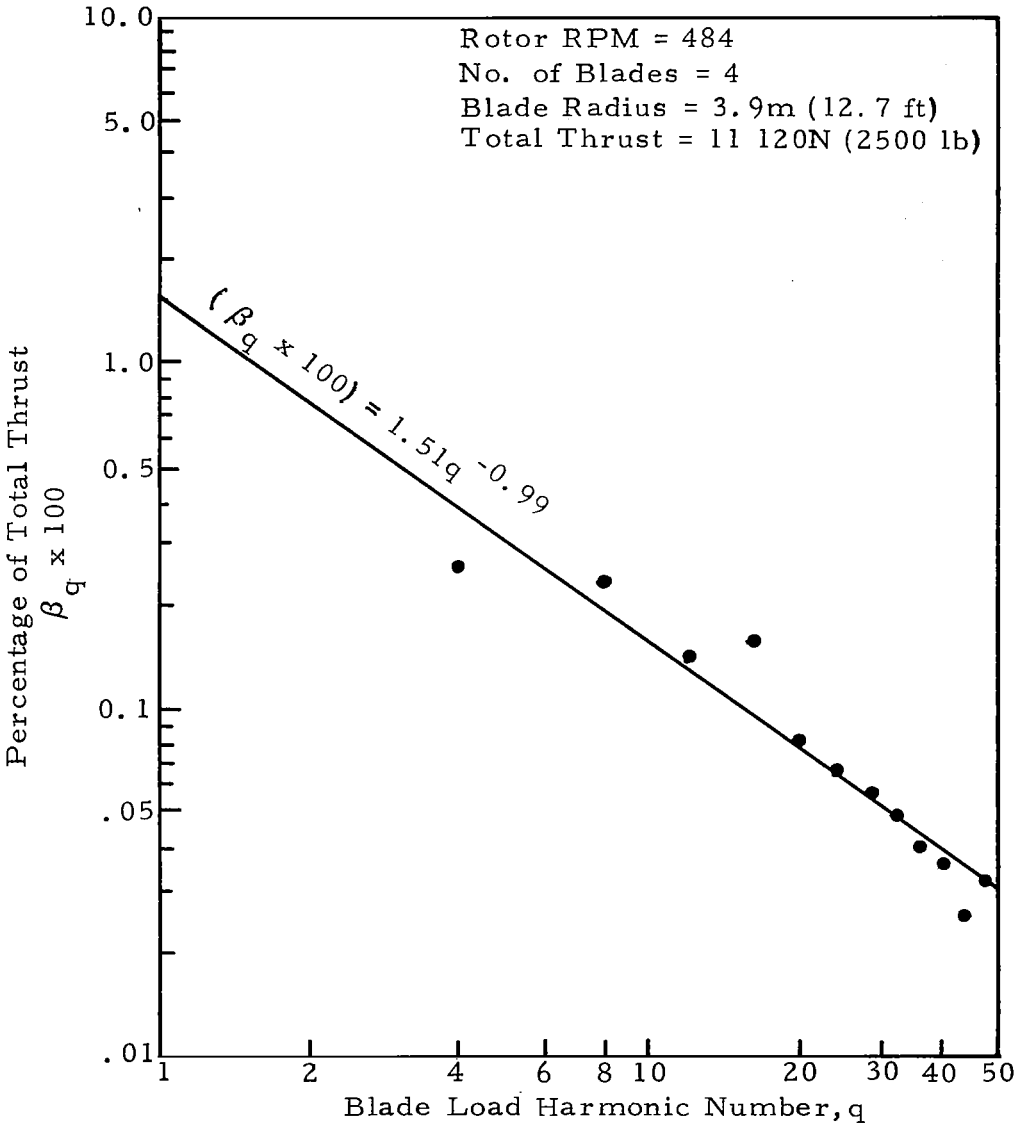

Figure 7. Calculated Blade-Load Harmonics;
Lunar Lander Test Series,
Hughes OH-6

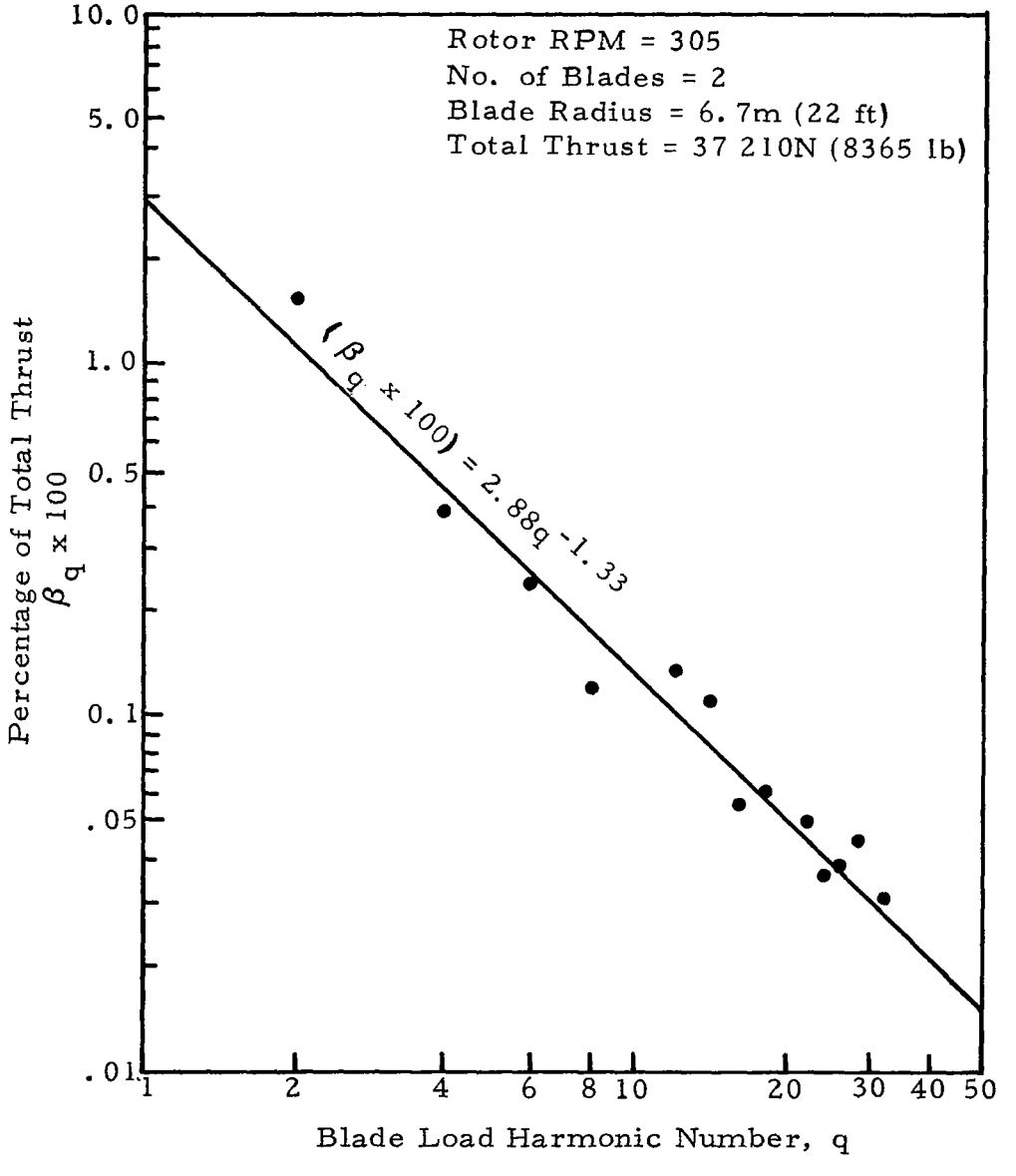

Figure 8. Calculated Blade-Load Harmonics;
Lunar Lander Test Series,
Bell 205 (Low Fuel)

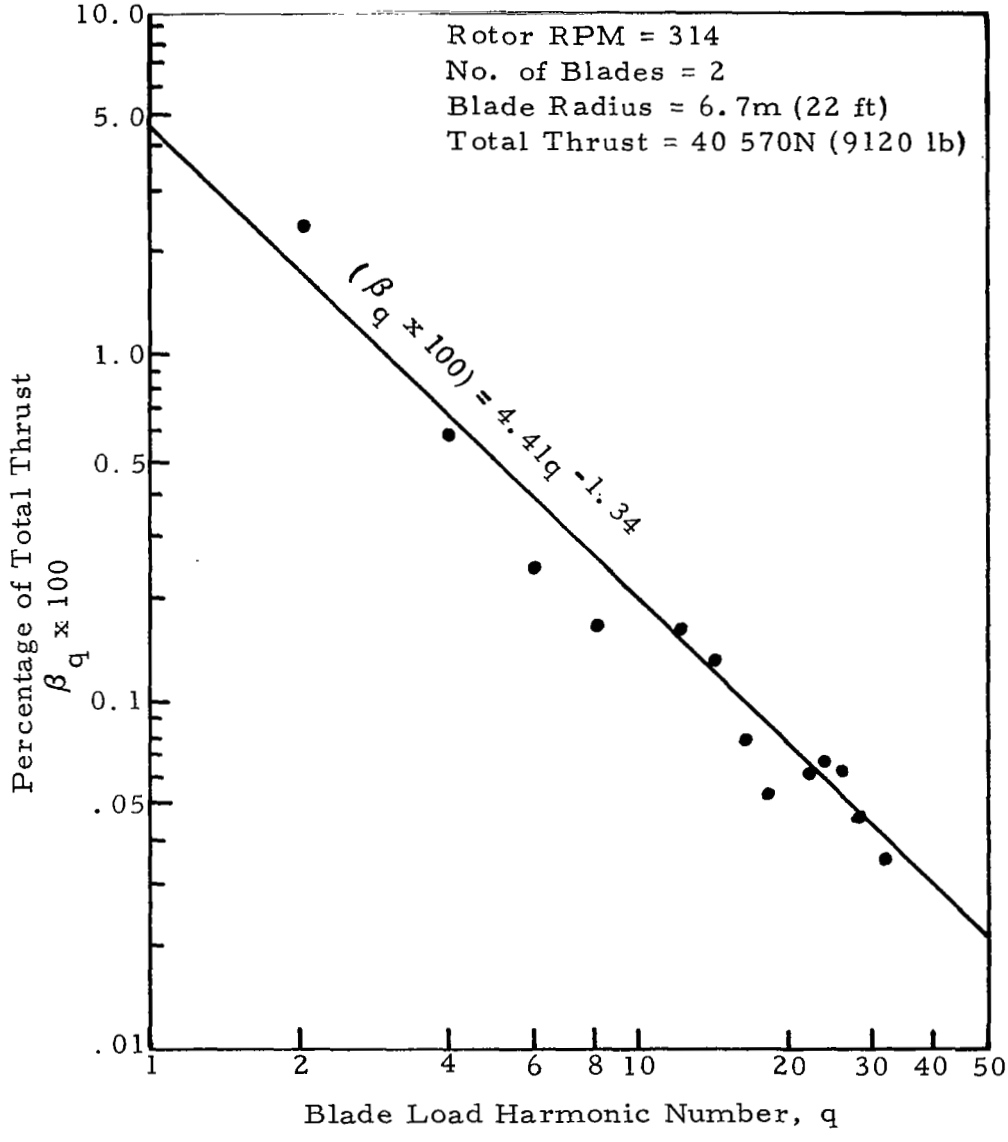

Figure 9. Calculated Blade-Load Harmonics;
Lunar Lander Test Series,
Bell 205 (Full Fuel)

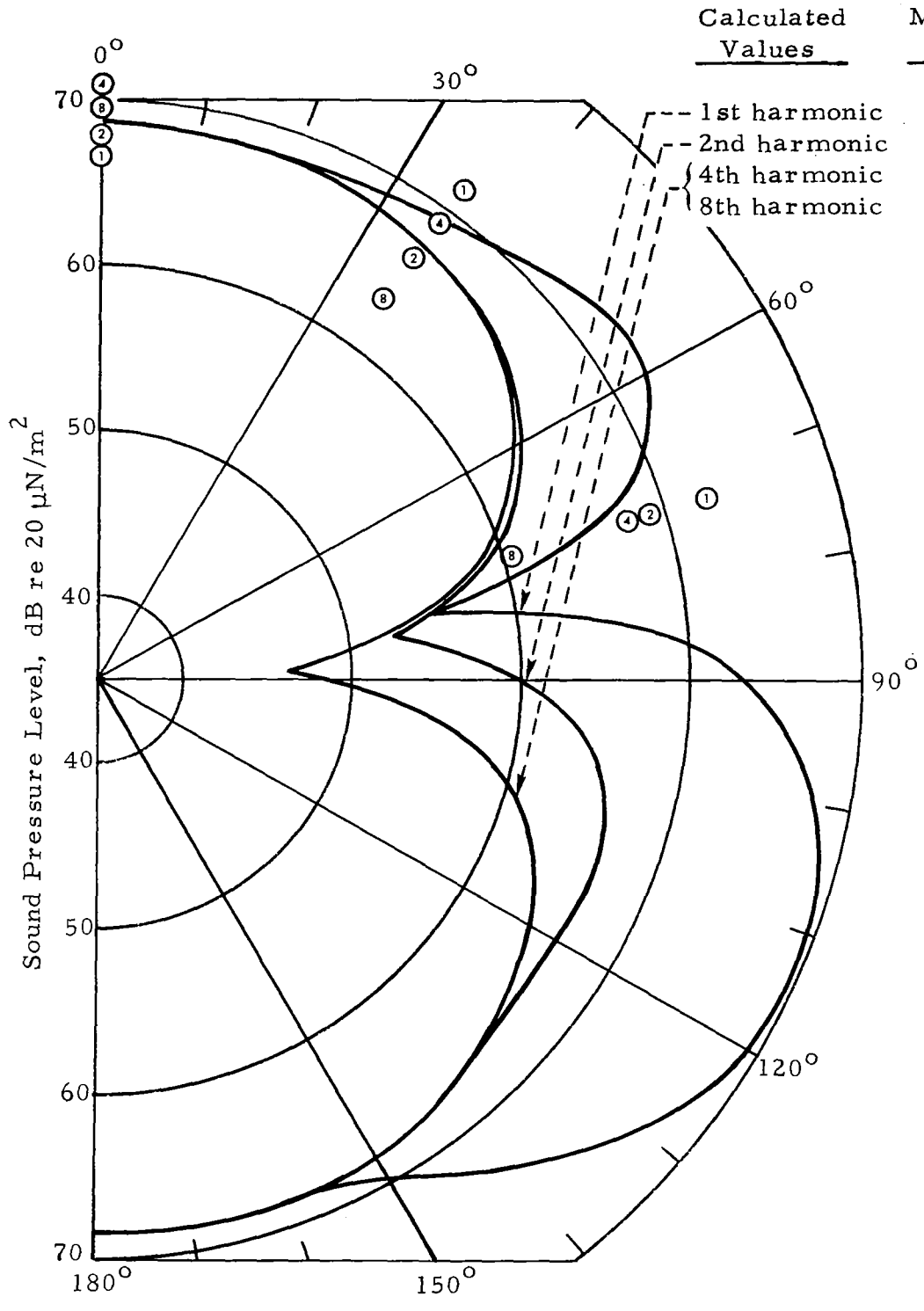

Figure 10. Calculated Directivity Pattern of Sound Harmonics with Comparison to Measured Values for Hughes OH-6, Lunar Lander Series

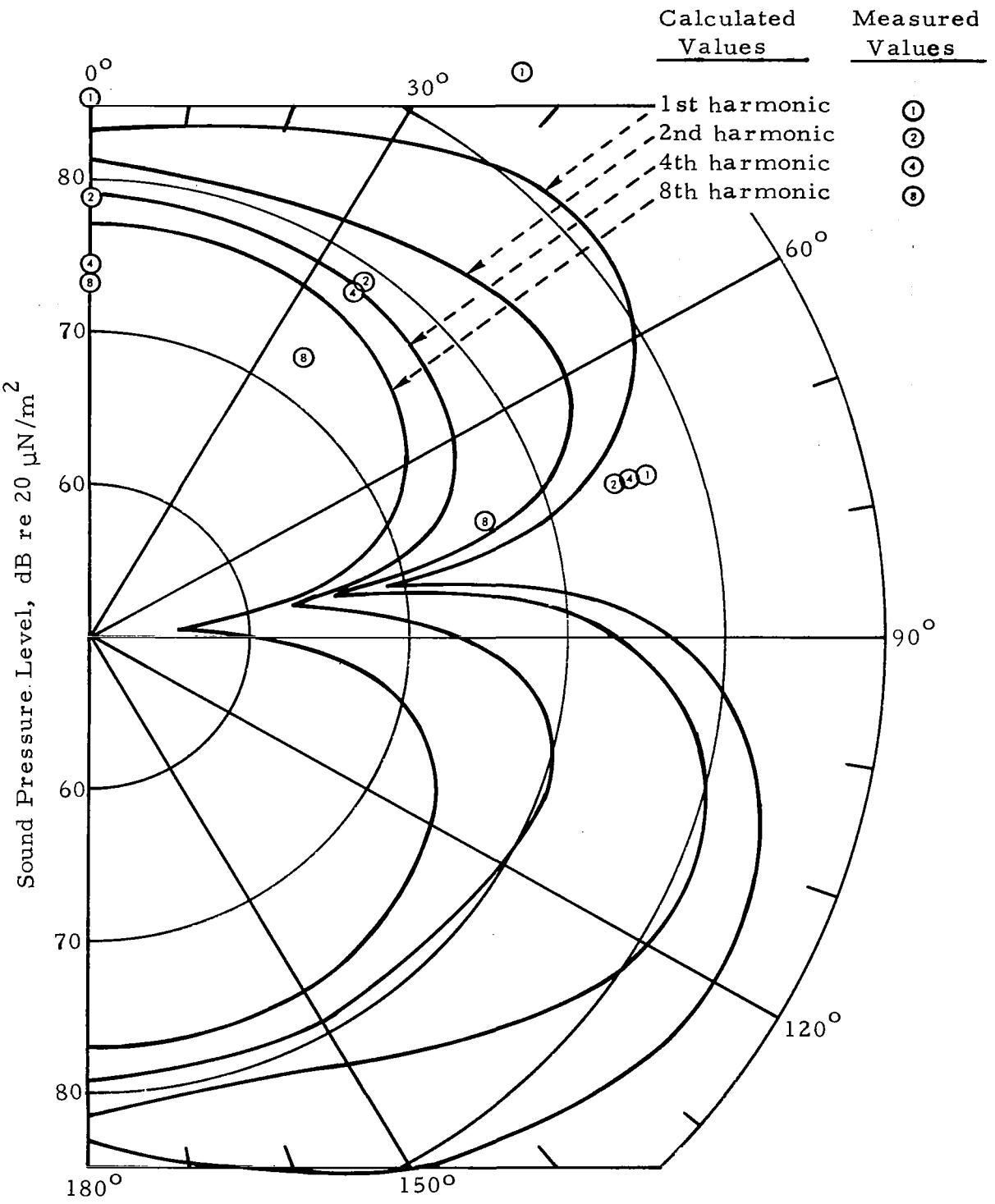

Figure 11. Calculated Directivity Pattern of Sound Harmonics with Comparison to Measured Values for Bell 205 (Full Fuel), Lunar Lander Series

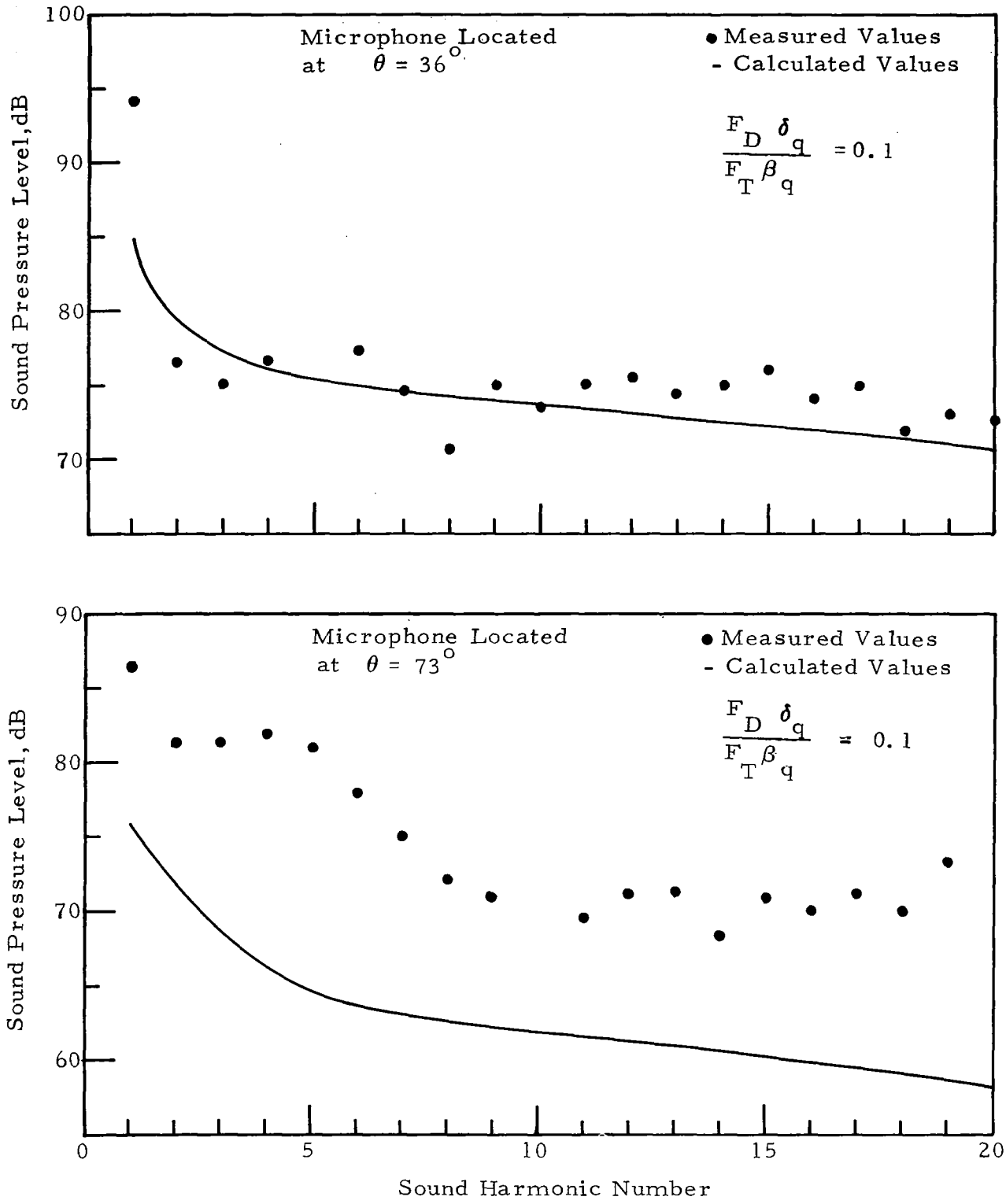

Figure 14. Comparison of Measured and Calculated Sound Harmonics for Bell 205, (Full Fuel); Lunar Lander Test Series

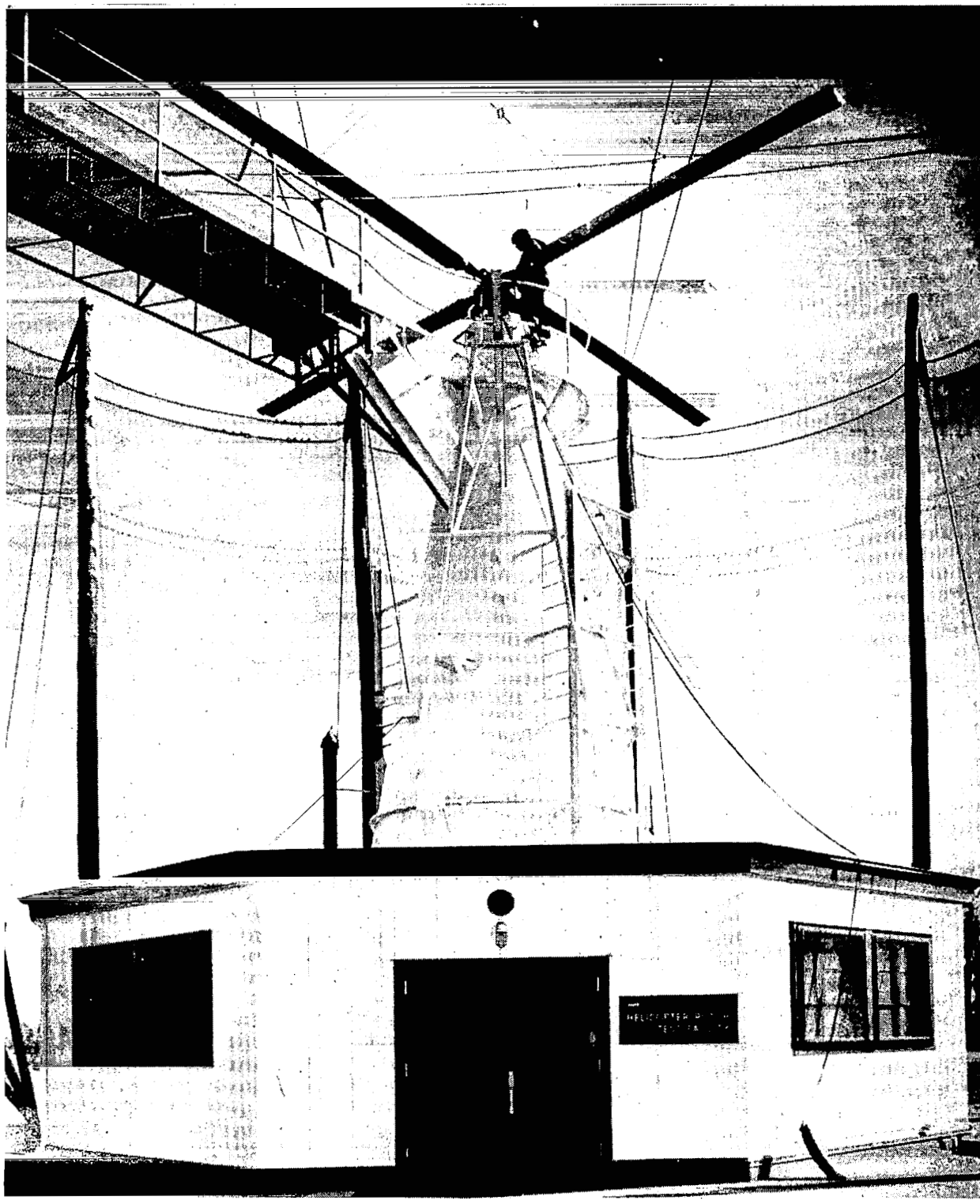

Figure 15. NASA Langley Research Center
Helicopter Rotor Test Facility

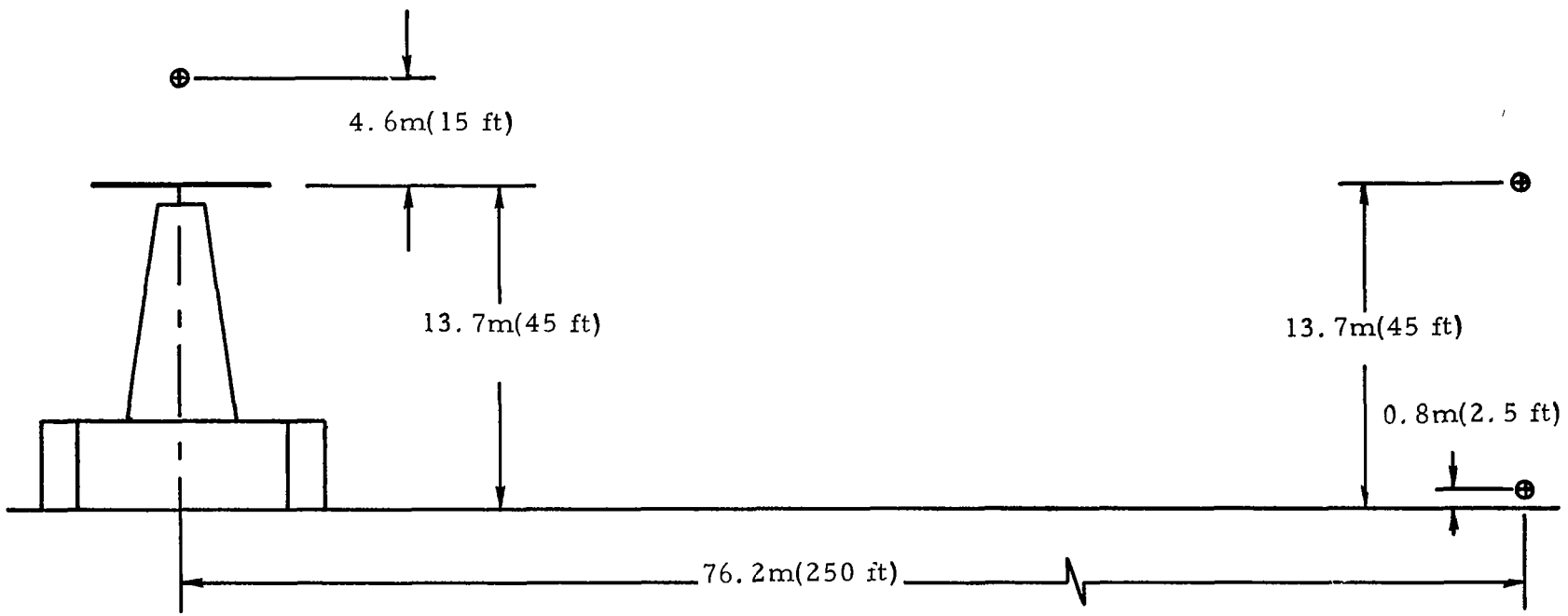

Figure 16. Microphone Locations for Rotor Tower Test 12-A

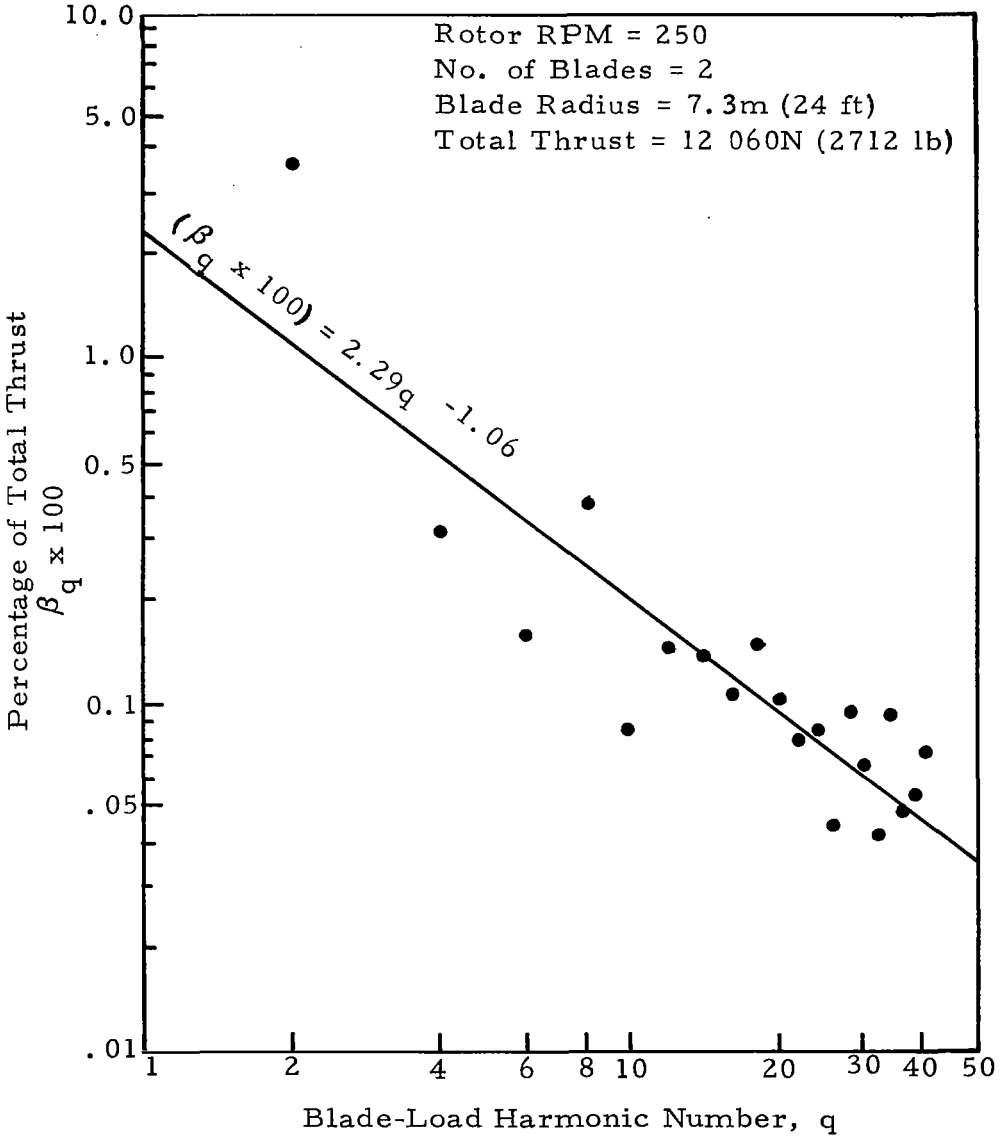

Figure 17. Calculated Blade-Load Harmonics: Rotor Tower Test 12-A, Run 104

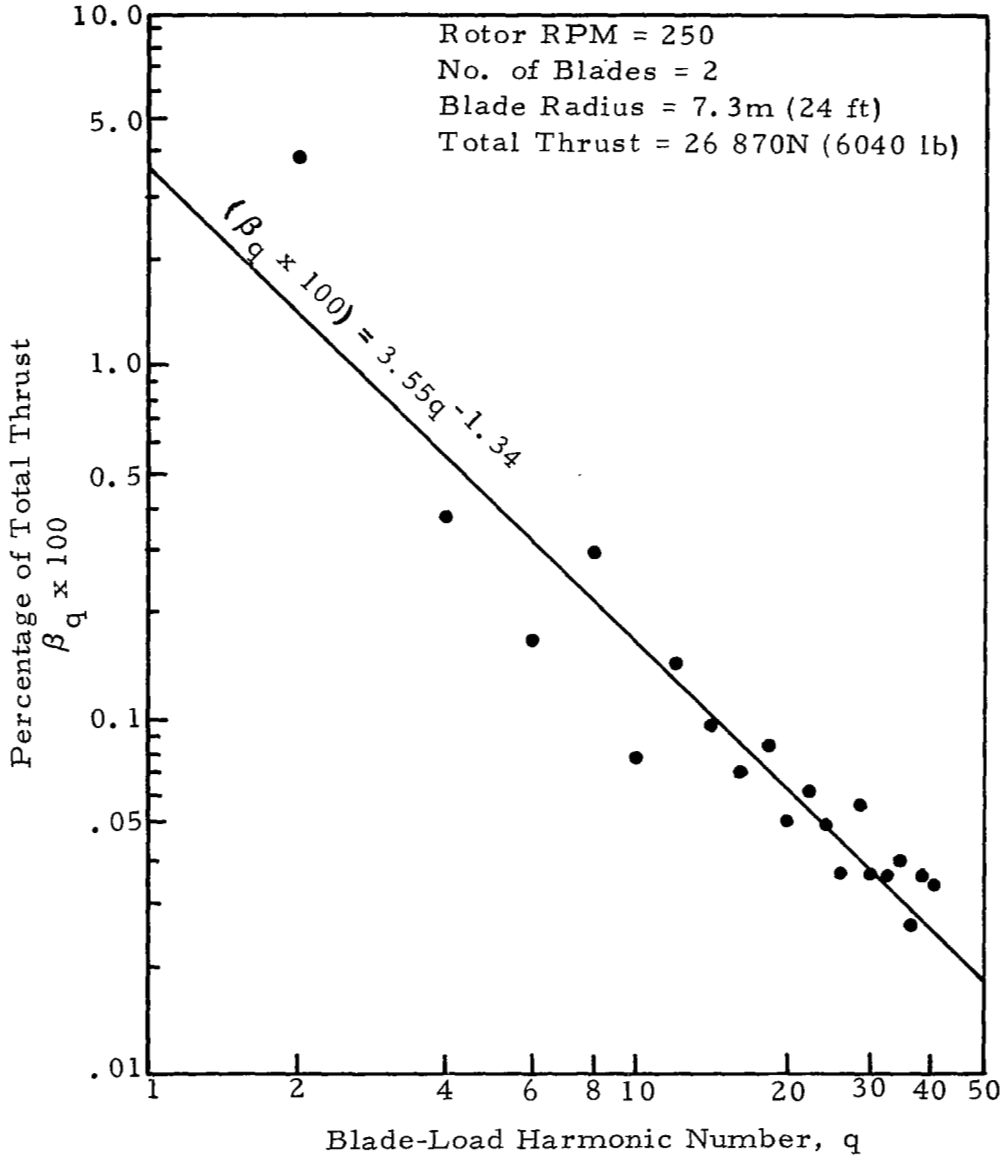

Figure 18. Calculated Blade-Load Harmonics: Rotor Tower Test 12-A, Run 109

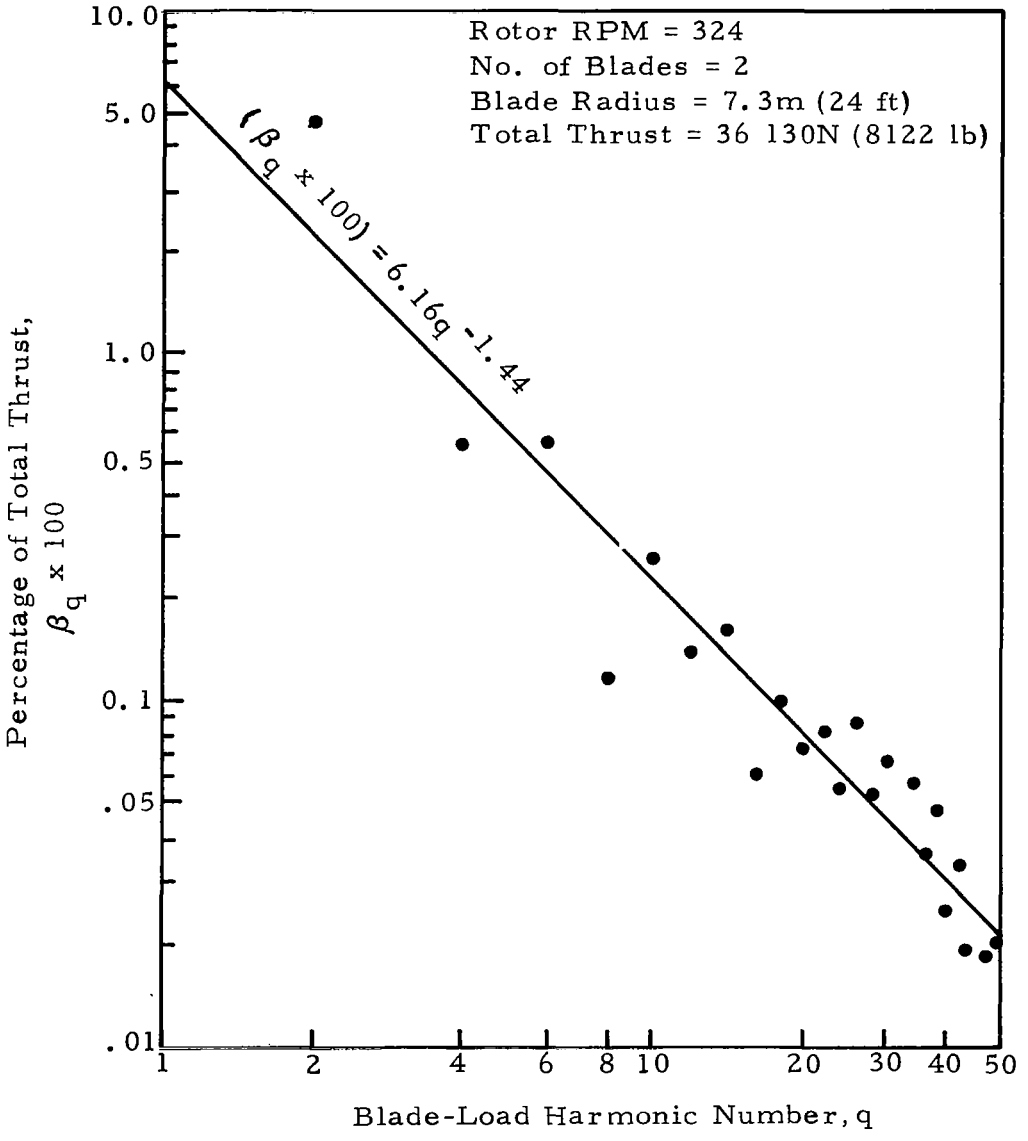

Figure 19. Calculated Blade-Load Harmonics: Rotor Tower Test 12-A, Run 112

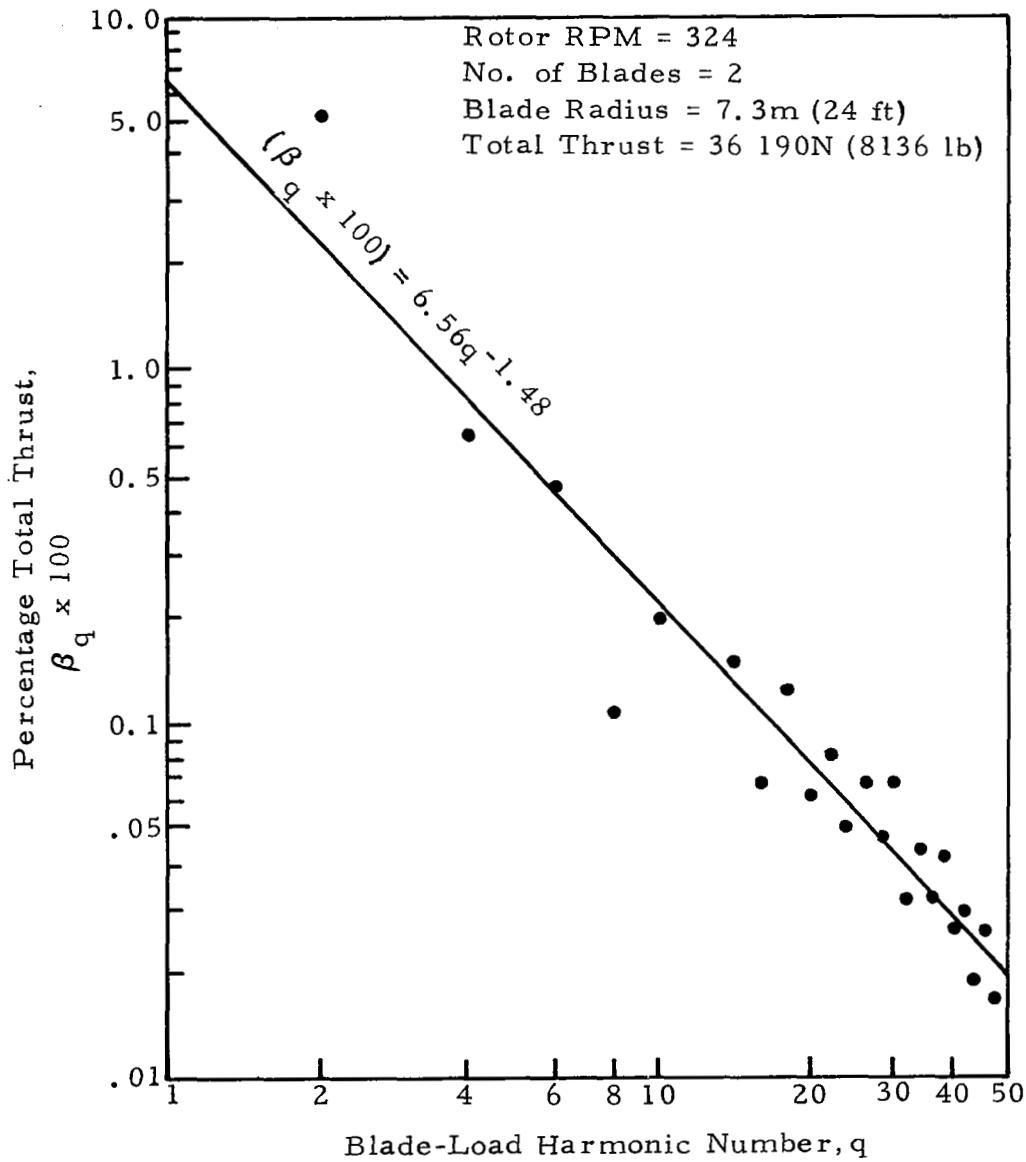

Figure 20. Calculated Blade-Load Harmonics: Rotor Tower Test 12-A, Run 114

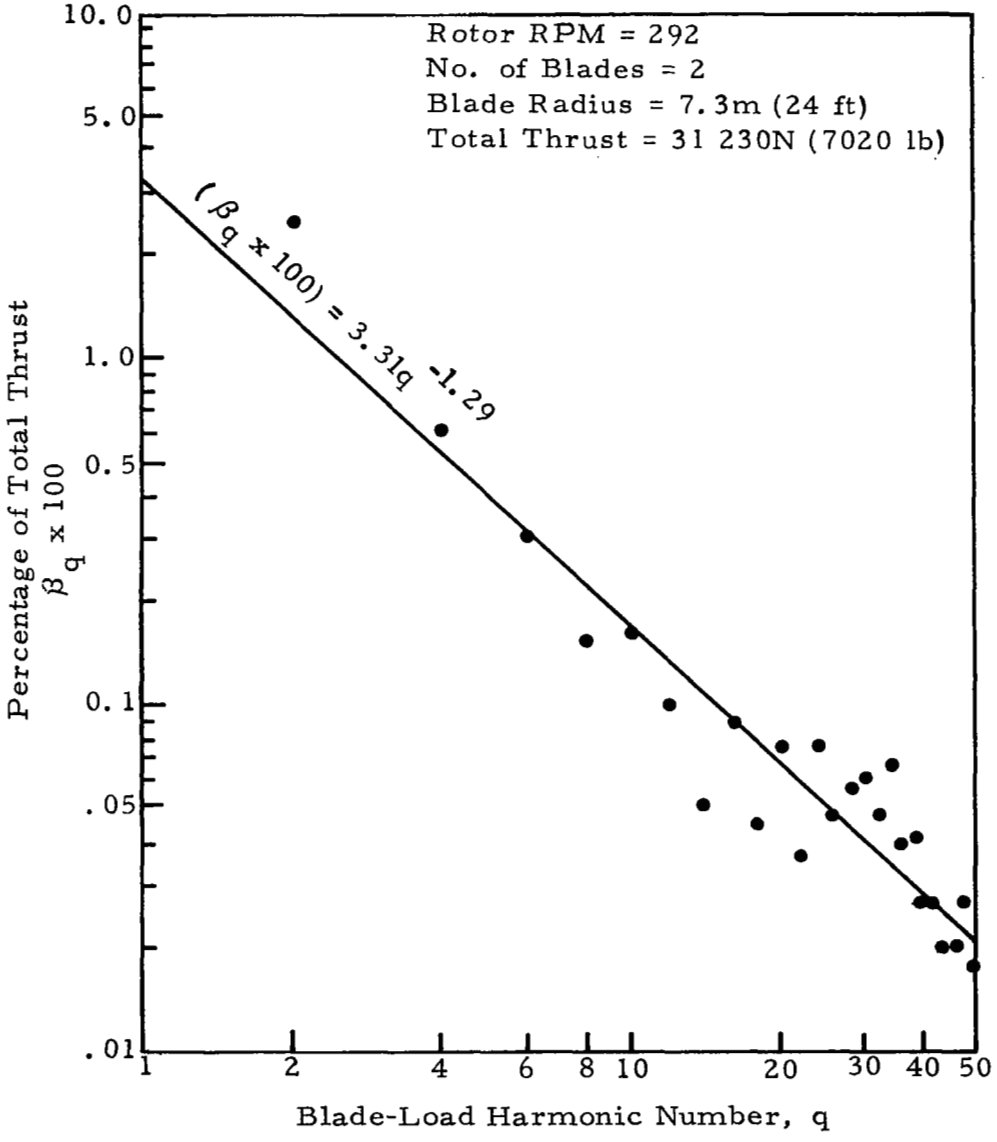

Figure 21. Calculated Blade-Load Harmonics:
Rotor Tower Test 12-A, Run 122

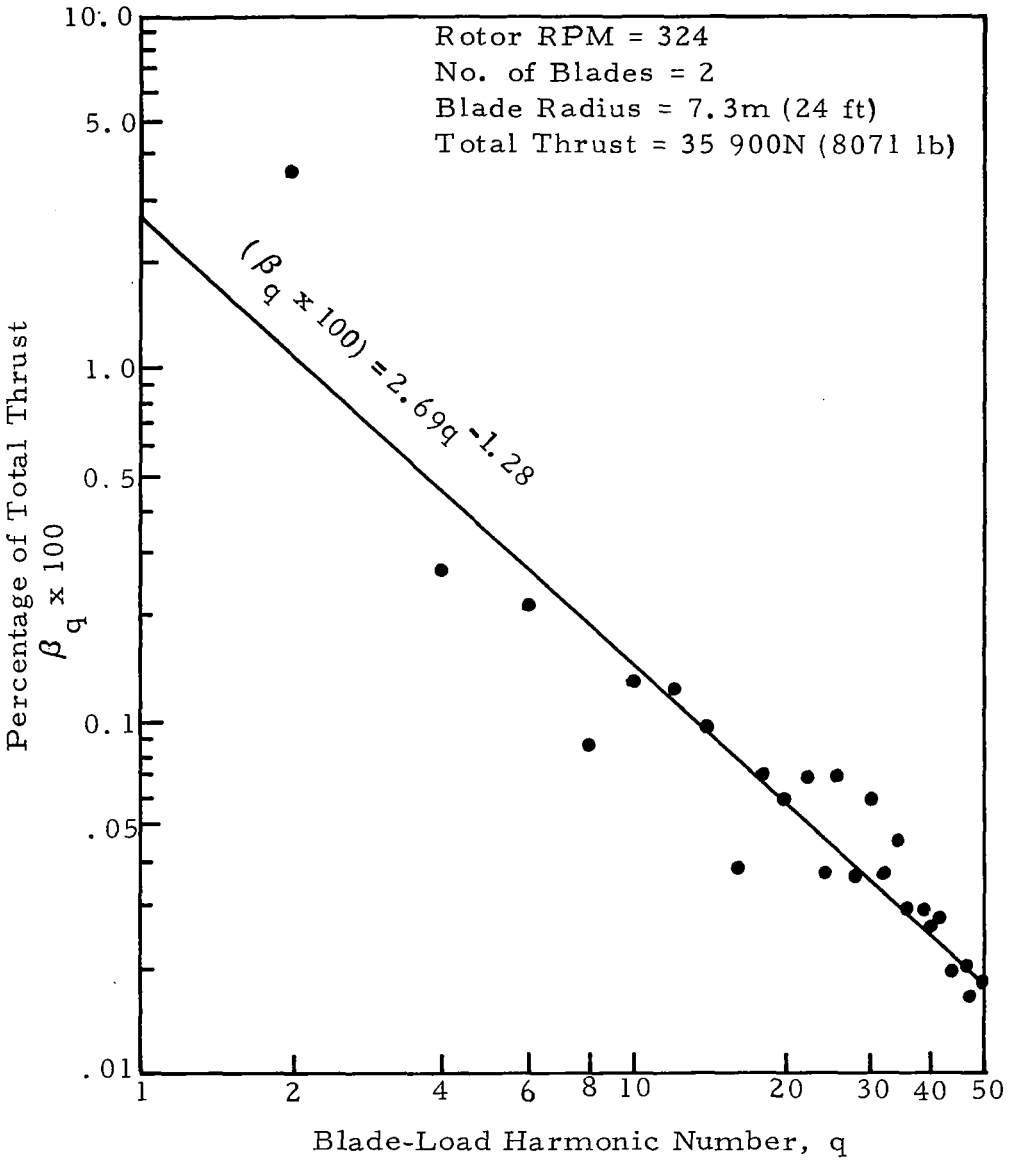

Figure 22. Calculated Blade-Load Harmonics: Rotor Tower Test 12-A, Run 126

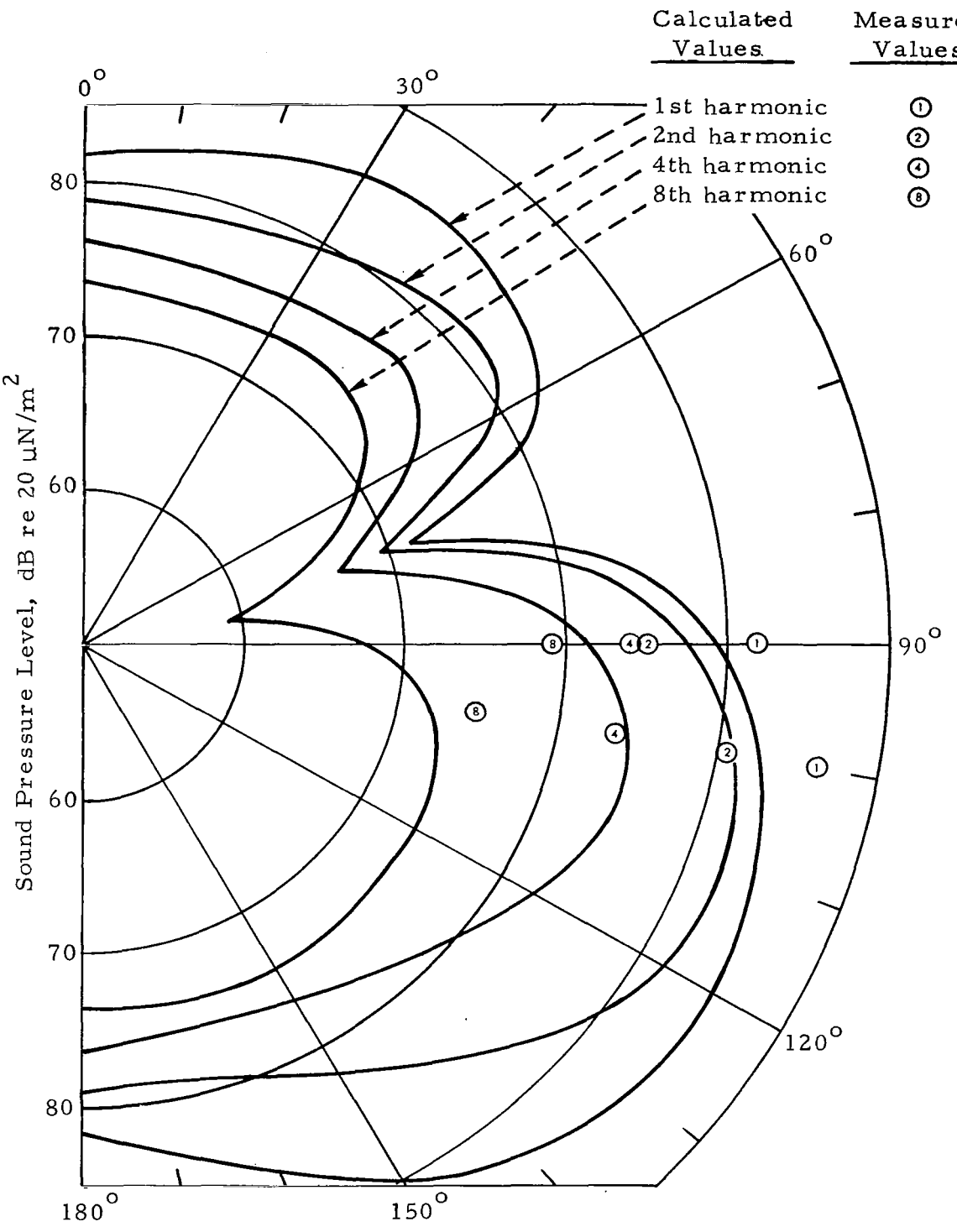

Figure 23. Calculated Directivity Pattern of Sound Harmonics with Comparison to Measured Values for Rotor Tower Test 12-A, Run 112

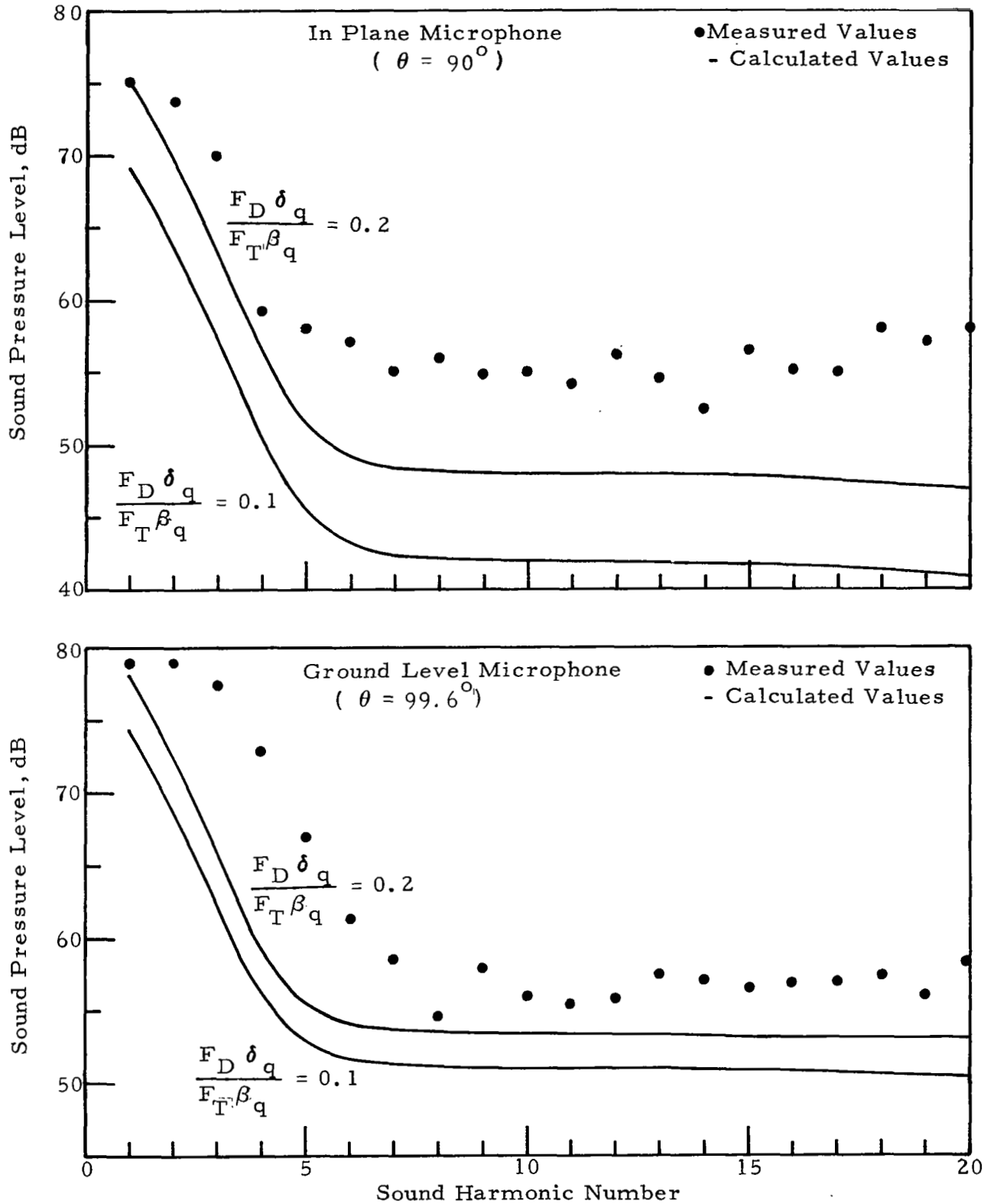

Figure 24. Comparison of Measured and Calculated Sound Harmonics for Rotor Tower Test 12-A, Run 104

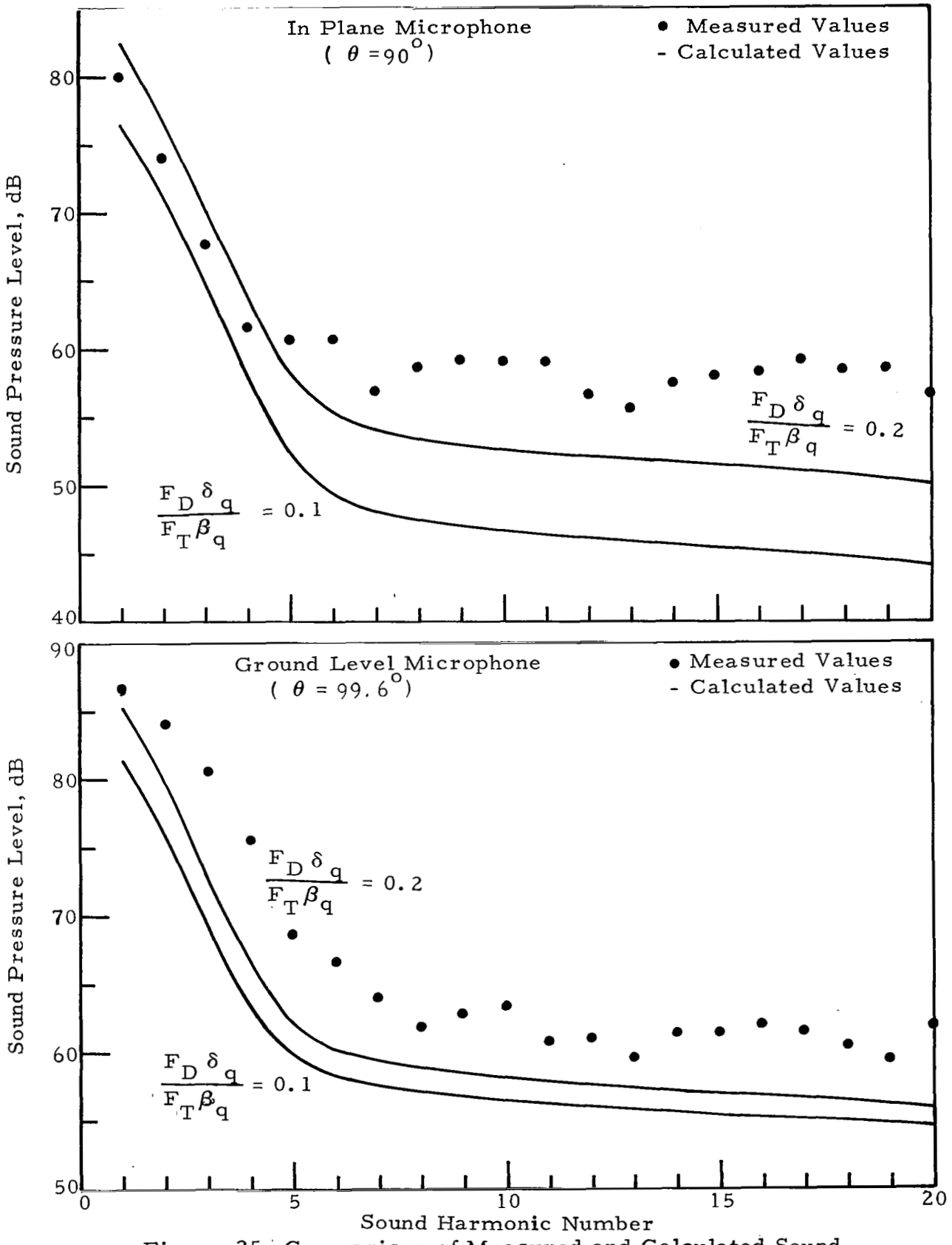

Figure 25. Comparison of Measured and Calculated Sound Harmonics for Rotor Tower Test 12-A, Run 109

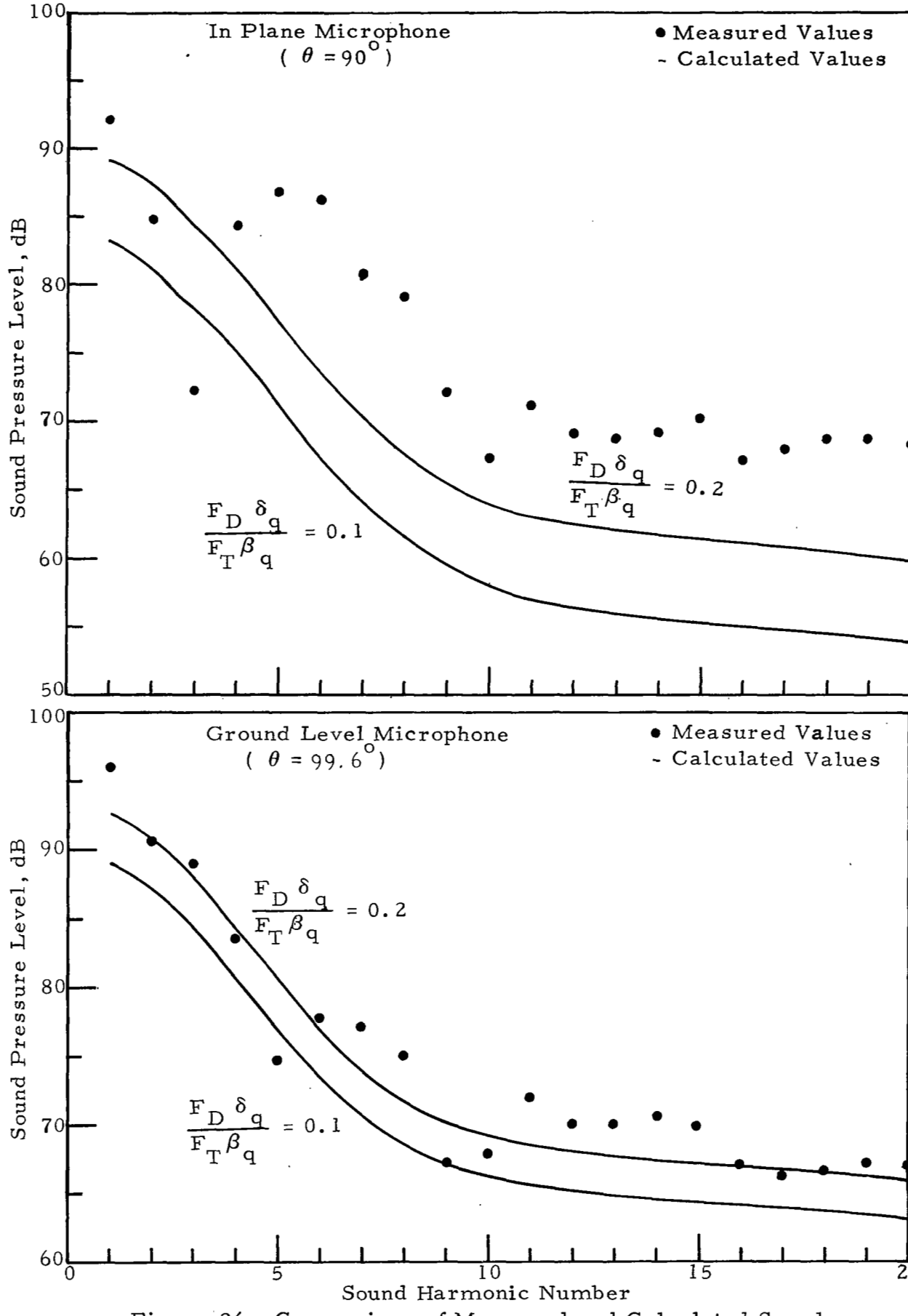

Figure 26. Comparison of Measured and Calculated Sound Harmonics for Rotor Tower Test 12-A, Run 112

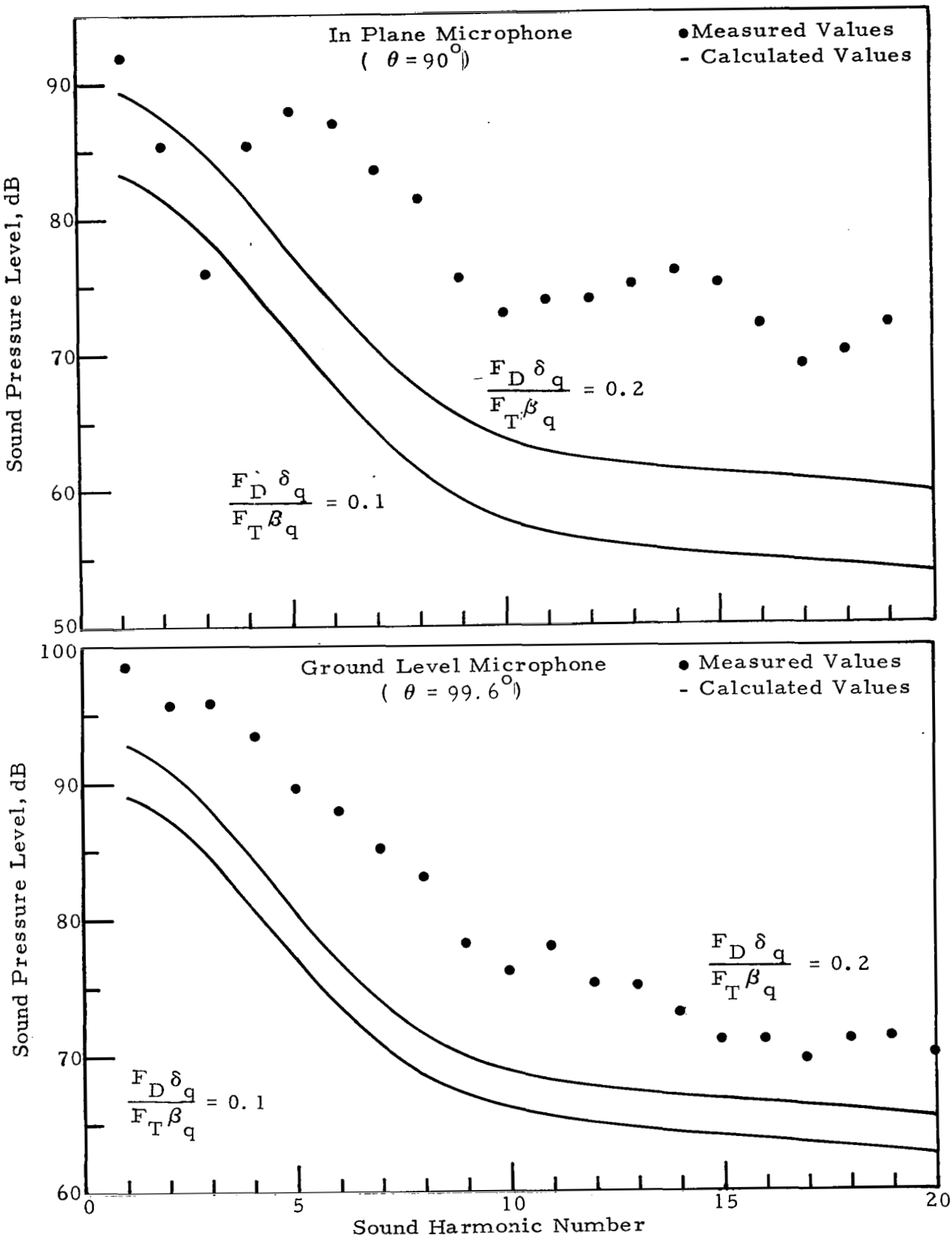

Figure 27. Comparison of Measured and Calculated Sound Harmonics for Rotor Tower Test 12-A, Run 114

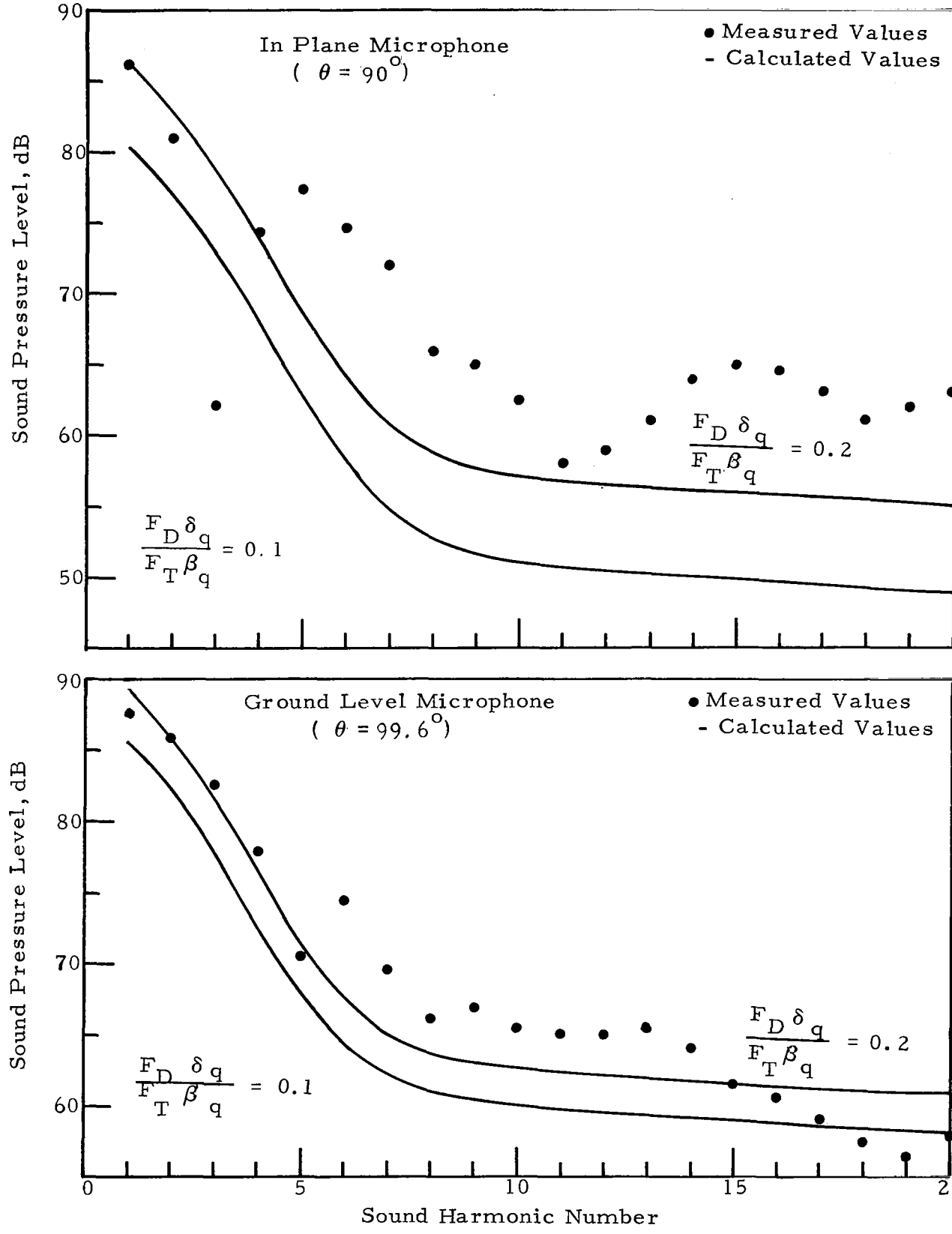

Figure 28. Comparison of Measured and Calculated Sound Harmonics for Rotor Tower Test 12-A, Run 122

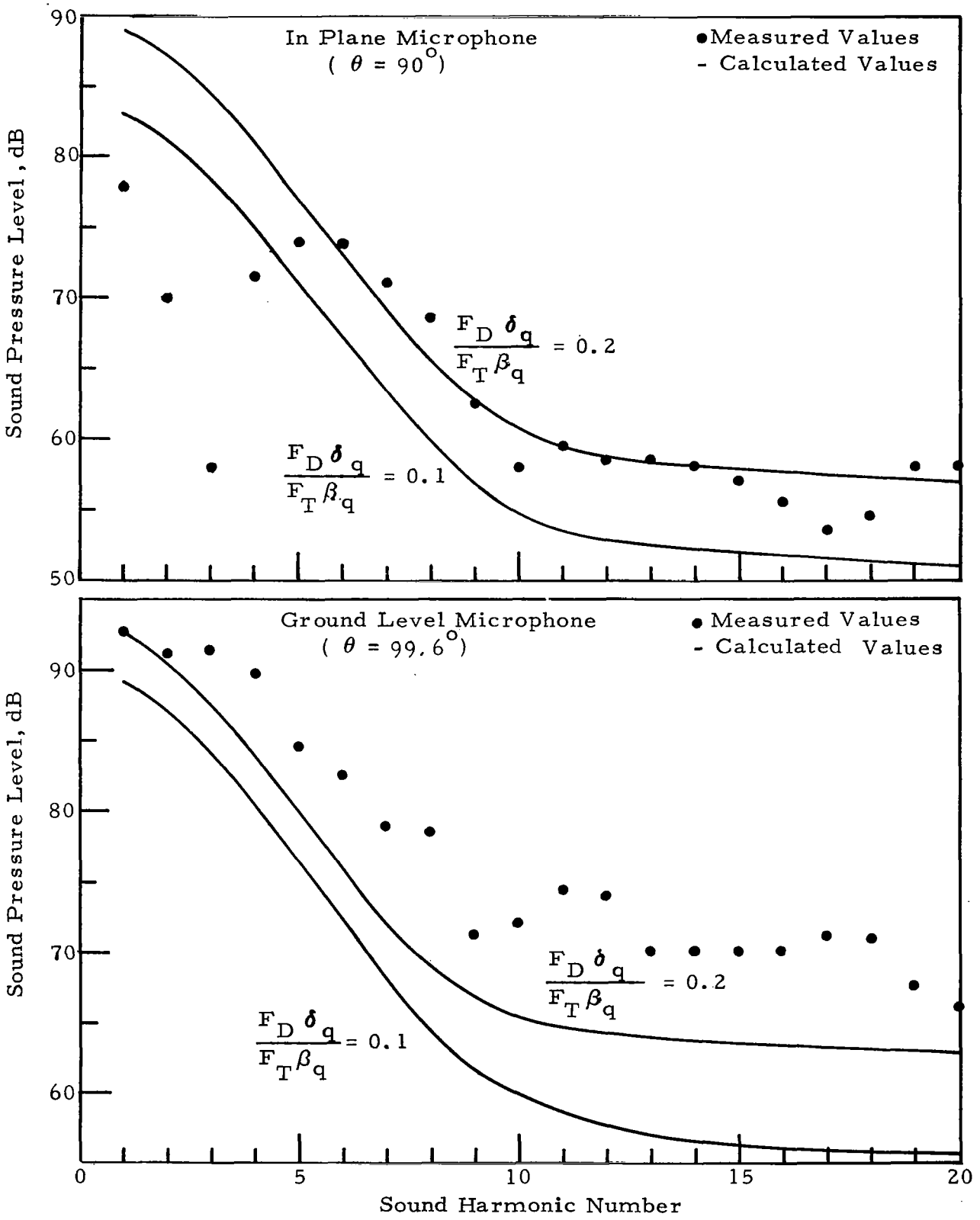

Figure 29. Comparison of Measured and Calculated Sound Harmonics for Rotor Tower Test 12-A, Run 126

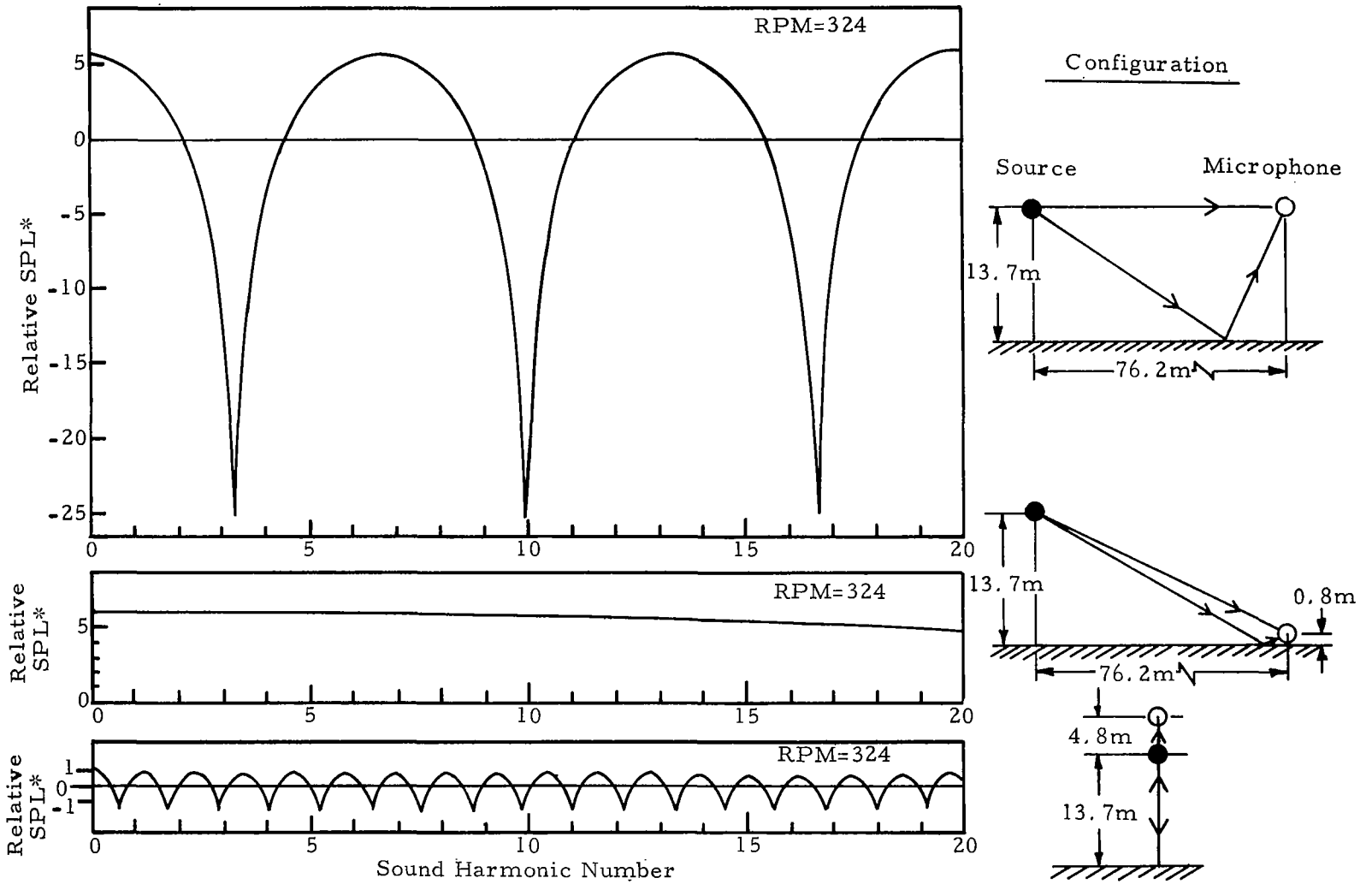

*SPL of combined direct and reflected sound relative to SPL from direct sound only.

Figure 30. Interference Pattern of Received Sound Pressure Level Due to Sound Reflection from Rigid Plane for Example Rotor RPM and Measurement Configurations